Master Thesis
The Performance of Photomultiplier for MEG Liquid Xe Calorimeter

Yasuko HISAMATSU

January 6th, 2005
February 4th, 2005 revised

Contents

Introduction

The quest for 'theory of everything' has long grabbed interests of physicists all over the world. Though we yet have a long way to go for this quest, a historic step toward 'theory of everything' was marked in the 20th century, known as the Standard Model. The Standard Model has been outstandingly successful in accounting for essentially all the data from laboratory experiments.

Entering the 21st century, we, a group of physicists and aggressive graduate students, have launched into a challenging search for new physics beyond the Standard Model. "MEG" is the name of our project, investigating Supersymmetric Grand Unified Theories (SUSY-GUT) through discovering a lepton-flavor-violating (LFV) decay $\mu^+ \to e^+\gamma$ with a sensitivity of 10^{-14}. Recent phenomenological studies on fundamental theories such as SUSY-GUT predicts that $\mu^+ \to e^+\gamma$ occurs with a decay branching ratio somewhere above 10^{-14}.[2] We therefore consider that we now have a good chance of making a discovery.

The MEG experiment will be conducted at Paul Scherrer Institut in Switzerland by using the πE5 beam line which provides the most intense DC muon beam in the world [1]. Not only the physics motivation but also detectors for the MEG Experiment have outstanding characteristics. The most notable will be liquid xenon calorimeter, a novel calorimeter for detecting γ rays with a 0.8m^3 volume of liquid Xe viewed by arrays of 830 photomultiplier tubes (PMTs). PMTs are operated in liquid xenon, a cold liquid whose temperature is 165K. Operating PMTs in such an environment is very difficult and challenging, and studies on performances of PMTs in liquid xenon are of great importance.

In this thesis, performance of PMT operated in liquid xenon is discussed. In chapter 1, the physics motivation of the MEG experiment and an overview of Liquid xenon Calorimeter is described. Here, requirements for PMTs are also discussed. R&D studies and performance test on PMT are described in chapter 2. In chapter 3, the R&D study on concrete design of the calorimeter front face is described.

Chapter 1

The MEG Experiment

1.1 Physics Motivation

In the MEG experiment,we search for the lepton flavor violating decay $\mu^+ \to e^+\gamma$. This decay mode is strictly forbidden in the framework of Standard Model. However, if supersymmetry is introduced, it will be within reach of laboratory experiments.

1.1.1 Standard Model and SU(5) GUT

The Standard Model is one of the great successes in the the twentieth century physics. It incorporates fundamental fermions by introducing the gauge bosons as mediators of interactions. In this theory, the interaction between the fundamental fermions, three pairs of quarks and three pairs of leptons, are mediated by gauge bosons $W^{\pm}$, Z^0, and γ of the electroweak sector, and the interaction between quarks are mediated by the gluons of the strong sector.
The electroweak sector is described by SU(2)⊗U(1) symmetry, where SU(2) corresponds to weak isospin, and U(1) to weak hypercharge. The strong interaction is described by SU(3) color symmetry. In this framework, quantities such as baryon number, lepton flavor and total lepton number are seen as symmetries and must be conserved, so that lepton flavor violating processes, such as $\mu \to e\gamma$ and $\tau \to \mu\gamma$, are strictly forbidden.
The SU(2)⊗U(1) gauge theory has been in impressive agreement with experiment. However, difficulties start to arise for the standard model when one attempt to unify the electroweak and strong interactions at some high unification energy, $E_{GUT} \sim 10^{16} GeV$, well above the electroweak scale. This problem is known as the hierarchy problem.
The first and simplest model of grand unification theory is the SU(5) model of Georgi and Glashow in 1974. They sought a "grand unified group G" where the SU(2)⊗U(1) electroweak symmetry and SU(3) color symmetry are embedded. And their solution was SU(5) which is spontaneously broken at very high energy scales.

$$G \supset SU(3) \otimes SU(2) \otimes U(1) \tag{1.1}$$

The SU(3)⊗SU(2)⊗U(1) gauge theory contains three independent gauge coupling constants. The Abelian U(1) coupling increases with energy, while the non-Abelian SU(2) and SU(3) coupling decrease with increasing energy. In the framework of SU(5) GUT, these couplings are expected to be extrapolated to common value at some energy. In the

precise measurements at the LEP collider, it was found that they do come close together at high energies, though not exactly at a point. The result of the extrapolation is shown in Fig.1.1.

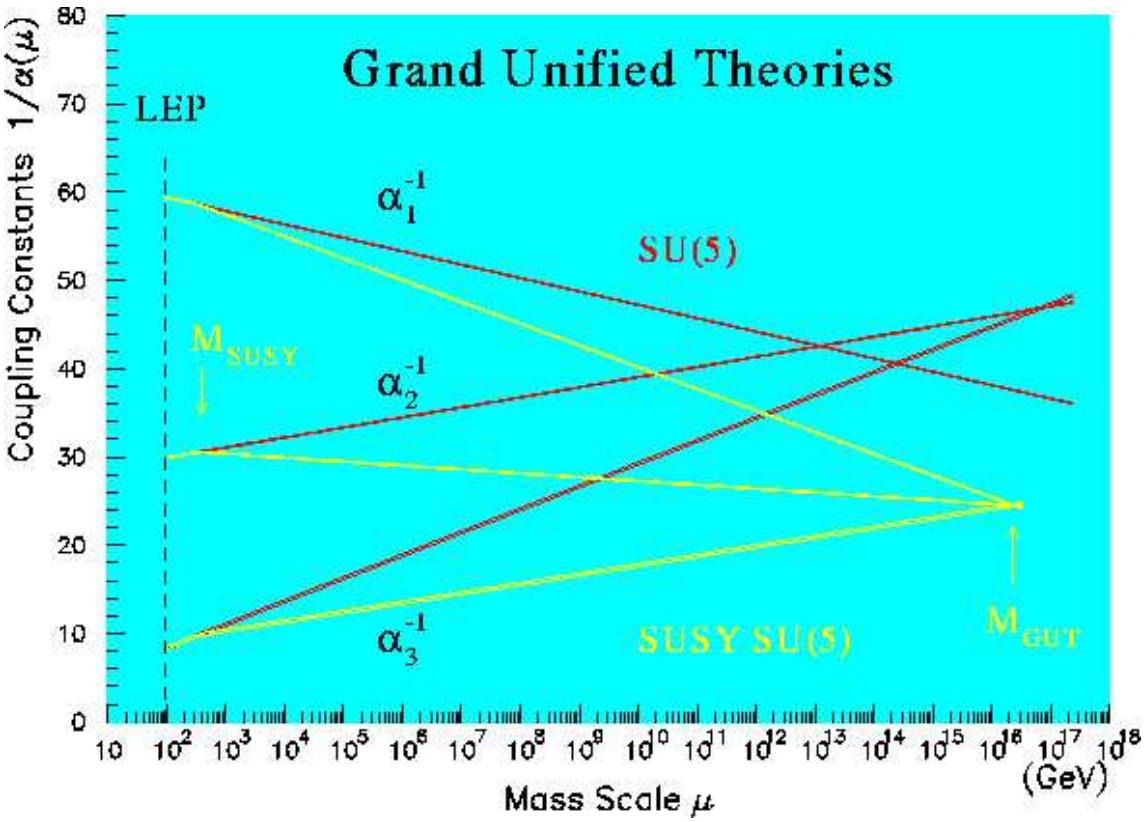

Figure 1.1: Extrapolation in energy of the coupling constants of SU(3)×SU(2)×U(1)

Here U(1), SU(2), SU(3) couplings are denoted by α_1, α_2, α_3 respectively. The general expression for the evolution is obtained by the renormalization group equation;

$$\alpha(q^2) = \frac{\alpha(\mu^2)}{1 + R\alpha(\mu^2)\ln(q^2/\mu^2)} \tag{1.2}$$

Here, R is given as

$$R = \frac{11n_b - 4n_f}{12\pi} \tag{1.3}$$

where $n_b = 0, 2$, and 3 for U(1), SU(2) and SU(3) respectively, and the number of the fermion generations $n_f = 3$.

1.1.2 Supersymmetric SU(5)

An elegant solution for the problem with the grand unification will be by supersymmetry. It is a symmetry that relates fermions and bosons, and links spin-$\frac{1}{2}$ Dirac matter fields with spin-1 bosonic gauge fields.
A generator of supersymmetry is an operator which transforms a bosonic state into a fermionic state, and vice versa. Such an operator, Q, must be an anticommuting spinor which carries half-integer spin, in the simplest case, spin 1/2. A Lorentz-covariant expression for this anticommutator is

$$\{Q, Q^\dagger\} = P^\mu \tag{1.4}$$
$$\{Q, Q\} = \{Q^\dagger, Q^\dagger\} = 0 \tag{1.5}$$
$$[P^\mu, Q] = [P^\mu, Q^\dagger] = 0 \tag{1.6}$$

where P^μ is a conserved vector quantity. Single-particle states of a supersymmetric theory fall naturally into irreducible representations of the supersymmetry algebra, called supermultiplets. Each supermultiplet contains both fermionic and bosonic states, which are known as superpartners of each other.
Thus supersymmetry introduces new elementary fermions and bosons, and these extra degrees of freedom reduce the slopes of α^{-1} dependence on $\ln(q^2/\mu^2)$ in Eq.1.2. Consequently, the three couplings α_1, α_2 and α_3 meet at a unique energy as shown in Fig.1.1.

1.1.3 Lepton Flavor Violation and SUSY-GUT

In the Standard Model, neutrinos are assumed to be in one helicity state, hence they are considered to be massless. As discussed in Sec.1.1.1, lepton flavor conservation is built in by hand with this assumption, strictly forbidding lepton flavor violation (LFV) processes. Recent measurements on atmospheric and solar neutrinos, however, have made breakthroughs, providing evidence for flavor oscillations, LFV in neutral current process and non-zero neutrino masses. By introducing of neutrino masses and their mixings into the Standard Model, it predicts unmeasurably small LFV in the charged lepton sector, whereas SUSY-GUT predicts LFV at a measurable level where additional sources of flavor mixing now come from sleptons. The LFV process, $\mu^+ \to e^+\gamma$, is thus enhanced in SUSY-GUT through loop diagrams shown in Fig.1.2.
LFV processes are thus specially sensitive to SUSY-GUT, and probing the LFV decay, $\mu^+ \to e^+\gamma$, is therefore a promising search for SUSY-GUT.

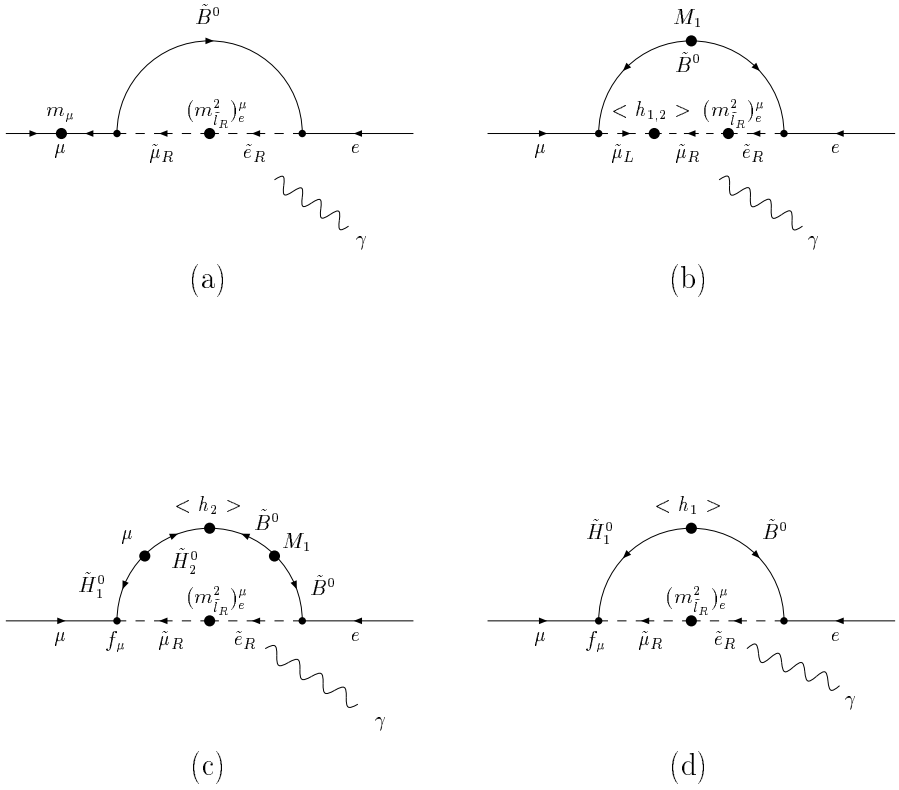

Figure 1.2: Diagrams of $\mu^+ \to e^+\gamma$ in SU(5) SUSY models

1.2 MEG Liquid xenon calorimeter

The calorimeter for the MEG experiment is a liquid xenon scintillation detector of "Mini-Kamiokande" type, which is a 0.8m^3 volume of liquid Xe viewed by arrays of 830 photo-multipliers (PMTs) from all sides. A schematic view of this detector is shown in Fig.1.3.

1.2.1 Liquid xenon as a scintillator

The origin of scintillation light from liquid xenon is de-excitation process of excited dimers of xenon, Xe_2^*. There are mainly two different processes for the de-excitation;

1. excitation process :

$$Xe + Xe^* \rightarrow Xe_2^* \rightarrow 2Xe + h\nu \tag{1.7}$$

2. recombination process :

$$Xe^+ + Xe \rightarrow Xe_2^+ \tag{1.8}$$
$$Xe_2^+ + e \rightarrow Xe^{**} + Xe \tag{1.9}$$
$$Xe^{**} \rightarrow Xe^* \tag{1.10}$$
$$Xe + Xe^* \rightarrow Xe_2^* \rightarrow 2Xe + h\nu \tag{1.11}$$

The wave length of the scintillation light emitted from these processes are in the vacuum ultra-violet (VUV), $178\pm5nm(FWHM)$, and the decay time constant is relatively short, 45nsec in the recombination process. The properties of liquid xenon are listed below (Table 1.1).
Liquid xenon has many advantages as a scintillator. The light yield is high, 75% of NaI(Tl), and the signal is fast, which enables accurate measurement with precise energy and timing resolutions. Its short decay-time is essential to minimize pile-up of high rate γ rays. Liquid xenon is free from a problem of non-uniformity, which enables construction of large homogeneous detector with a large acceptance.

Table 1.1: Properties of Liquid xenon

Atomic Number	54
Mass Number	131.29
Density	2.95g/cm^3
Boiling and meting point	165K, 161K
Triple point (temperature, pressure, density)	161K, 0.805atm, 2.96g/cm^3
Energy per scintillation photon(52.8MeV γ)	23.7eV
radiation length	27.7 mm
decay time	4.2nsec, 22nsec
decay time (recombination)	45 nsec
scintillation light wave length	178 $\pm$ 5nm (FWHM)
refractive index	1.61

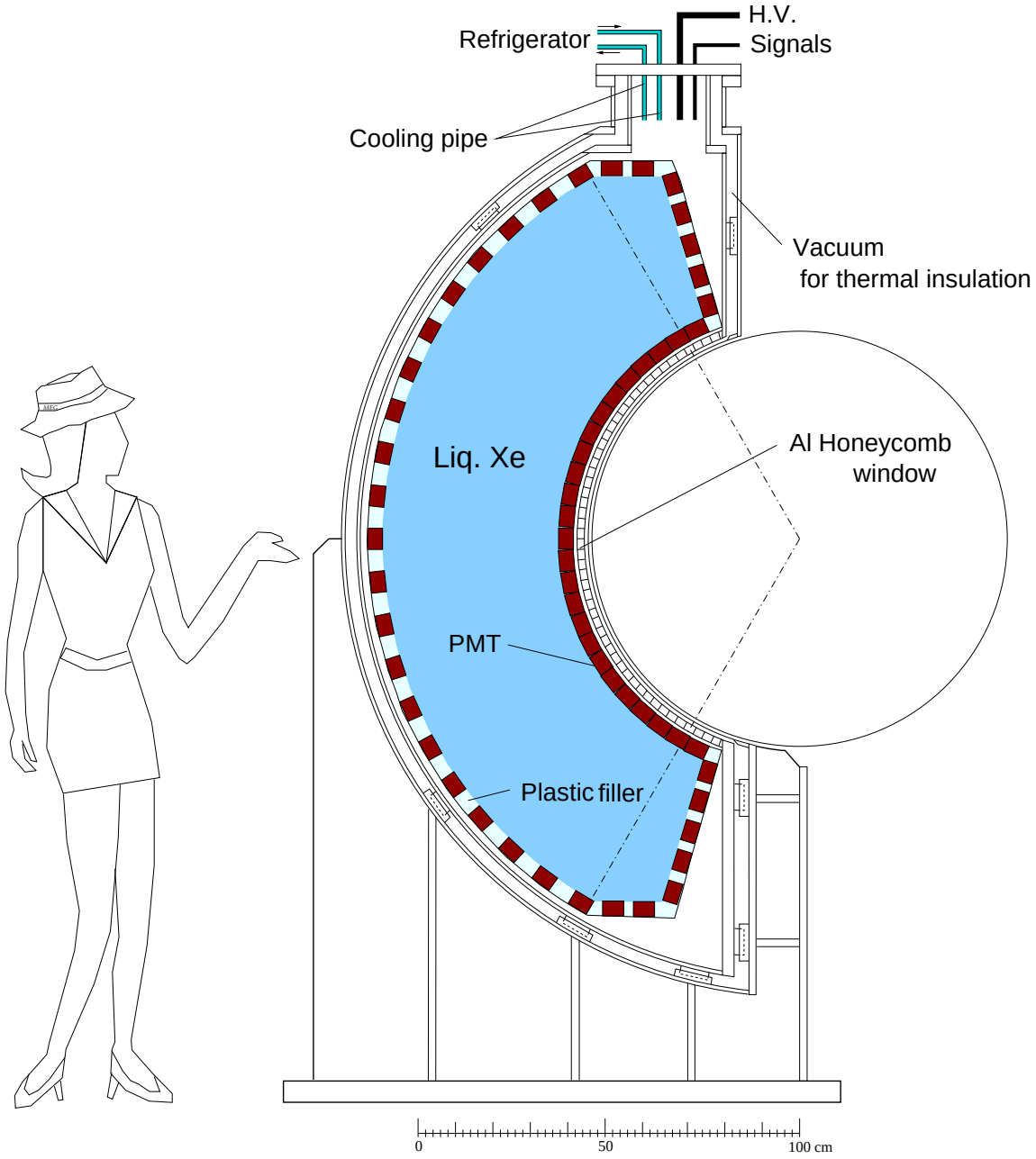

Figure 1.3: A cut view of the liquid xenon calorimeter

1.2.2 "mini-Kamiokande" Type and photomultiplier

Scintillation light from liquid xenon is detected by arrays of 830 PMTs located on all walls of the calorimeter in the liquid without any transmission window. This characteristic scheme, which is similar to that of Kamiokande, has an advantage of detecting a sufficient amount of scintillation light directly with many photomultipliers simultaneously with a fast response with a large active volume, compared to a segmented scintillation detector.
Thus, direct detection of scintillation light by PMTs is of great advantage. However, operating PMTs in liquid xenon is quite a difficult task. Requirements for PMTs operational in liquid xenon are as follows;

- Operational in $165K$, liquid xenon temperature, with high quantum efficiency (Q.E.) $\sim 10\%$

  Since PMTs are immersed in liquid xenon, they should be operational at $165K$, which is too cold for ordinary PMTs. Nowadays, the bialkali photocathode is popular in particle physics experiments for its low dark current and high sensitivity, but its high electrical resistivity at low temperature has long been an obstacle to its use in low temperature. Fig.1.4 shows the temperature dependence of sheet resistance of various photocathode materials [3]. Because of this high sheet resistance, charge supply to the photocathode takes about 0.01 sec after emission of photoelectrons. Therefore, the photocathode runs short of electrons, which results in the deterioration of signal outputs of PMT. Fig. 1.5 shows temperature dependence of PMTs with various photocathode [3].
  The higher the photoelectron yield is, the better performance of the detector can be easily achieved. Therefore it is necessary for PMT to keep high quantum efficiency even at 165K, which may not be easy due to the high sheet resistance of photocathode as described above.

- Sensitive to VUV light

  Since the wave length of liquid xenon is in vacuum ultra-violet region, photomultiplier must be sensitive to that wavelength, which is too short for ordinary PMTs to detect.
  A choice of window material of PMT needs consideration since it tends to absorb the VUV light. The short wavelength limit is determined by the ultraviolet transmittance of the window material.

- Short PMT length

  The front face of the calorimeter where γ rays pass should have long radiation length so as not to let γ rays deposit their energy. Therefore, thickness of the front face must be minimized. While, PMTs are placed all sides of liquid xenon calorimeter, including the front face where γ rays enter. Consequently, the length of PMTs should also be reduced.
  In addition, it is also necessary to place the detector to minimize its volume in

order to place the calorimeter close to a target, which helps to enlarge the detector acceptance. In minimizing the detector volume, we needs to reduce the length of PMT.

- Operational under magnetic field

  Liquid xenon calorimeter will be placed in the magnetic field at a level of 50 Gauss. This magnetic field is generated by the positron spectrometer which consists of magnets placed in the vicinity of the calorimeter. Needless to say, PMTs inside the calorimeter will be exposed to this magnetic field.
  In general, gain of PMT is affected by external magnetic field because the electron trajectories are influenced by the magnetic field and photoelectrons cannot be precisely focused onto the first dynode. The effects of external magnetic field, however, can be reduced by choosing a proper dynode structure.
  In selecting dynode structure of PMT in the MEG experiment, such considerations must be done.

- Consideration on TTS

  Liquid xenon calorimeter is expected to achieve a good timing resolution. The intrinsic timing resolution of PMT, in other words, transit time spread of PMT should also be minimized.

- Consideration on withstanding pressure

  During an operation of the liquid xenon Calorimeter, the pressure inside the calorimeter could rise up to 0.2MPa. Therefore, PMT must withstand this pressure.

- Reduction of heat load from PMT base

  Since 830 PMTs are immersed in liquid xenon, the heat emanating from their base circuit must be minimized to reduce heat load in the liquid xenon. Therefore, the high resistance should be used in the base.

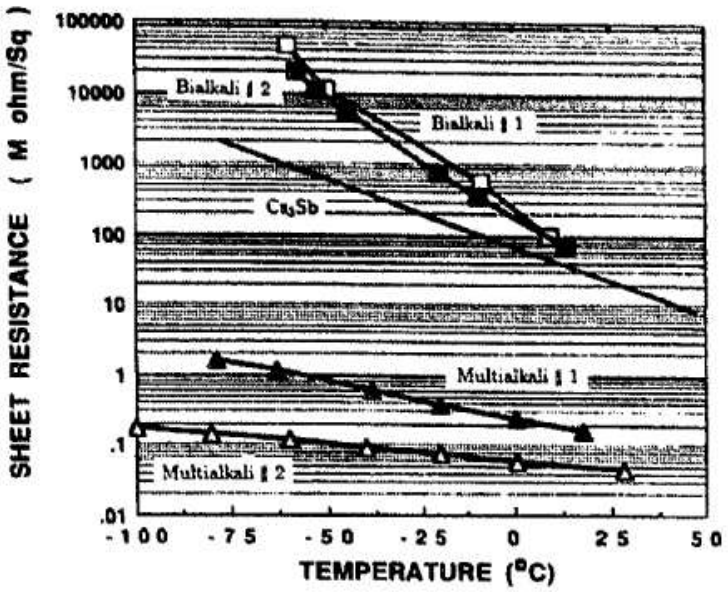

Figure 1.4: Sheet resistance of different photocathode as a function of temperature[3]

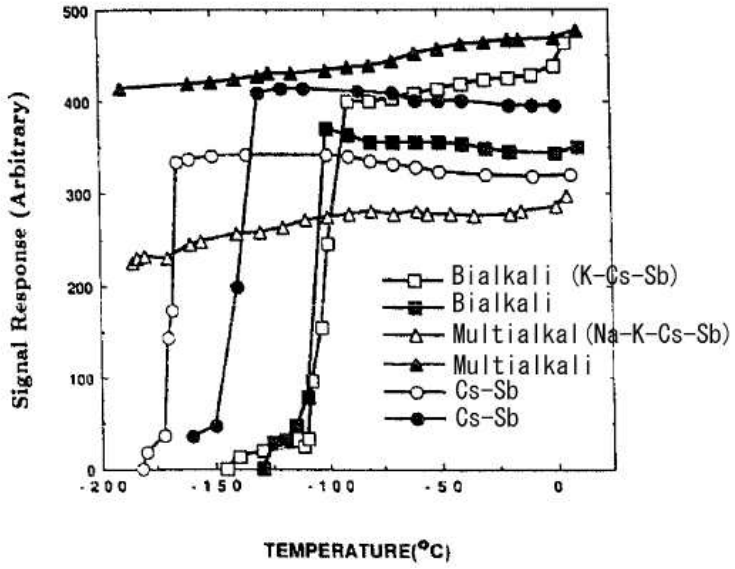

Figure 1.5: The temperature dependence of signal output for PMTs using various photocathode [3]

Chapter 2

Photomultiplier for the MEG Experiment

2.1 R&D works on Photomultiplier

Continuous efforts to develop Photomultiplier(PMT) for the MEG Experiment has been made in collaboration with Hamamatsu Photonics Inc., and three versions of PMTs have been developed so far.
For the first version PMT, we employed Rb-Cs-Sb as photocathode material, taking advantage of its comparatively low surface resistance at 165K. With 228 first version PMTs, large prototype detector of the liquid xenon calorimeter was constructed. A schematic view of the large prototype detector is shown in Fig.2.4. The first version PMTs are placed onto the rectangular box inside the detector whose active volume is 67 liters. With this prototype detector, various tests on PMT were performed, proving a long-term stability of first version PMT and its adequate quantum efficiency for the MEG experiment, approximately 6%, even at low temperature.
The second version PMT employs K-Cs-Sb and has ten aluminum strip patterns on its photocathode. Though surface resistance of K-Cs-Sb at low temperature is relatively high compared to that of Rb-Cs-Sb, the aluminum strip pattern works to reduce the resistance greatly, so that the quantum efficiency of the second version PMT is expected to increase dramatically. The photocathode of final version PMT is the same as that of second version PMT, K-Cs-Sb, and has 22 aluminum strip patterns on its photocathode. Three versions of PMT are shown in Fig. 2.1 ,Fig. 2.2, and Fig. 2.3

Figure 2.1: First Version

Figure 2.2: Second Version

Figure 2.3: Final Version

These PMTs, which will be immersed in liquid xenon, has some characteristic features; In order to operate PMT at 165K, liquid xenon temperature, the heat load from their base circuit is minimized. The circuit diagram is shown in Fig.2.5. The body of PMT is

made of metal, which enables PMT to withstand pressure up to 0.3 MPa. Since there is no electric potential difference between the body of PMT and the photocathode, PMT is operated with the photocathode grounded and the high positive voltage. The metal channel dynode structure of the PMTs helps to reduce the length to be 32 mm and assures the stability under external magnetic fields. As wavelength of xenon scintillation light ranges over 178 ± 5nm,the vacuum ultraviolet region, PMT widow is made of quartz glass, which transmits VUV light.
The properties of PMT are summarized in Table 2.1 and their features and characteristics are summarized in Table 2.2.

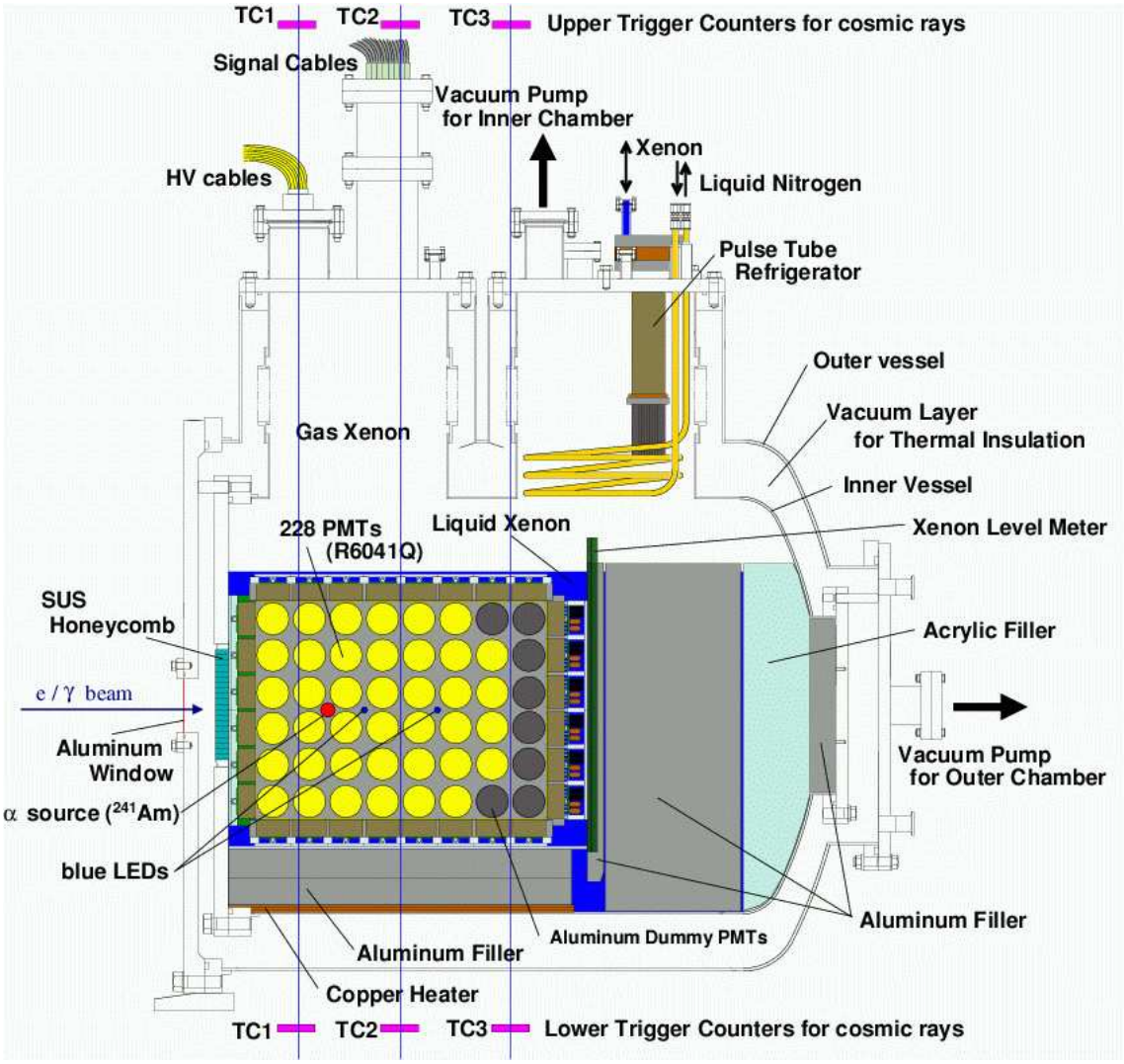

Figure 2.4: The large prototype detector

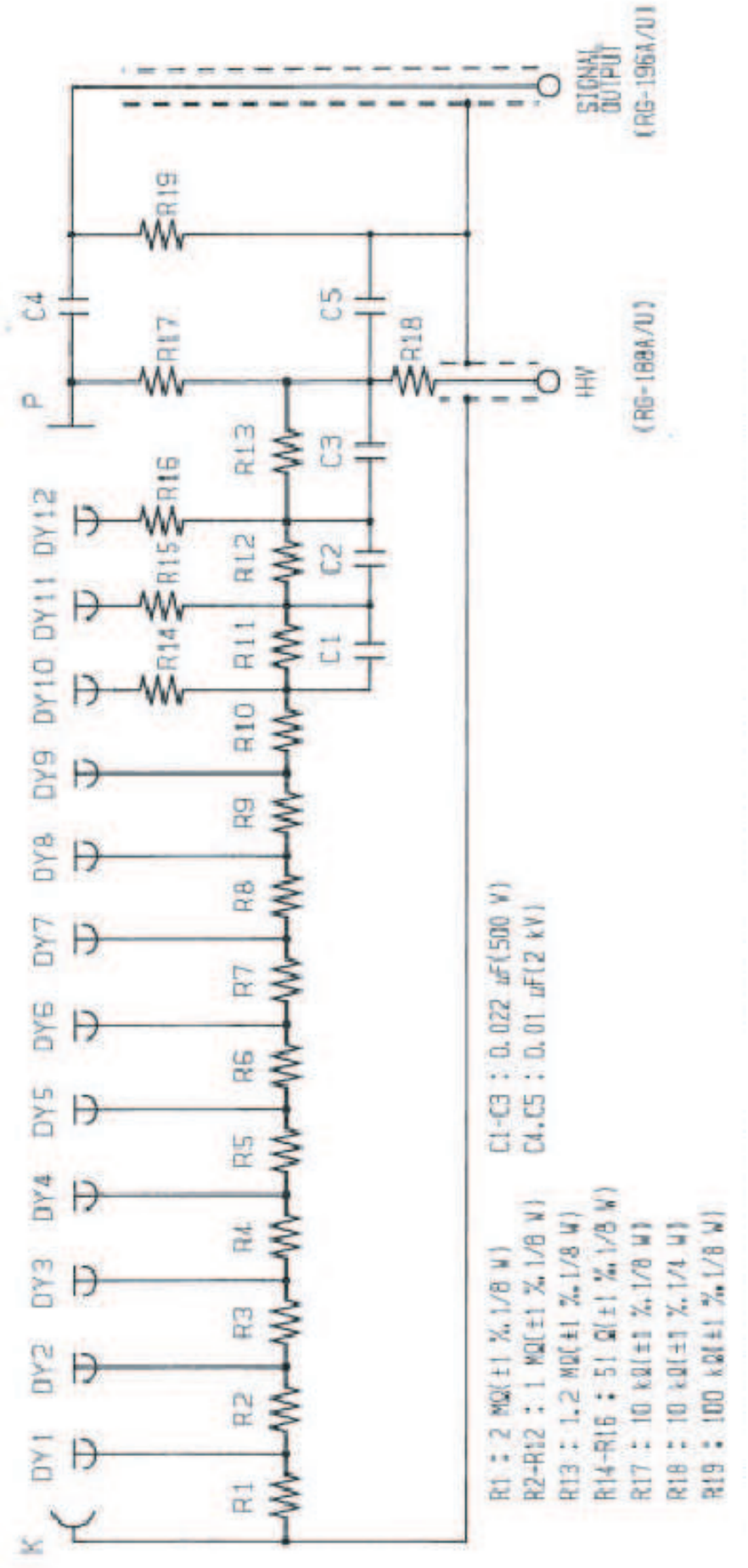
SIGNAL OUTPUT
(RG-196A/U)
(RG-188A/U)
HV
P
K
C4
C5
R19
R17
R18
R16
R15
R14
R13
R12
R11
R10
R9
R8
R7
R6
R5
R4
R3
R2
R1
C3
C2
C1
DY12
DY11
DY10
DY9
DY8
DY7
DY6
DY5
DY4
DY3
DY2
DY1
R1 : 2 MΩ(±1 %, 1/8 W)
R2-R12 : 1 MΩ(±1 %, 1/8 W)
R13 : 1.2 MΩ(±1 %, 1/8 W)
R14-R16 : 51 Ω(±1 %, 1/8 W)
R17 : 10 kΩ(±1 %, 1/8 W)
R18 : 10 kΩ(±1 %, 1/4 W)
R19 : 100 kΩ(±1 %, 1/8 W)
C1-C3 : 0.022 μF(500 V)
C4,C5 : 0.01 μF(2 kV)

Table 2.1: Properties of PMT for MEG experiment

	First Version PMT	Second Version PMT	Final Version PMT
Type No.	R6041Q	R9288	R9288
photocathode	RB-Cs-Sb	K-Cs-Sb	K-Cs-Sb
Aluminum Strip Pattern	0	10 strips	22 strips
PMT Size	57mm ϕ		
Size of effective area	46mm ϕ		
Dynode type	Metal channel		
Number of stages	12		
Typical HV	1000 V		
amplification with 1000V	$\sim 9 \times 10^6$		

Table 2.2: Characteristics of PMT for MEG experiment

Features	Advantages for MEG experiment
Photocathode material	Sensitive to VUV, High Q.E. even at 165K
Aluminum Strip Pattern	Reduction of sheet resistance of photocathode
Quartz glass as PMT window	Transmission of VUV light
Metal Package	Able to withstand pressure up to 0.3 MPa
metal channel dynode structure	Reduction of PMT length
high resistance value in PMT base circuit	Reduction of heat load

In October 2003, a gamma ray beam test was conducted using πE1 beam line at Paul Scherrer Institut in order to examine the response of the large prototype detector where 228 first version PMTs were installed. Gamma rays from π^0 decays ($\pi^0 \to \gamma\gamma$) produced in the charge-exchange process ($\pi^- + \mathrm{p} \to \mathrm{n} + \pi^0$) were used. An unanticipated problem showed up during this beam test, namely a large decrease of PMT output when PMTs were cooled down and the beam was on. Fig.2.6 shows the time dependence of PMT output from 5.5MeV alpha source as a function of the time after the beam was turned on. This alpha source is attached inside the detector wall and can be regarded as constant point-like light source.

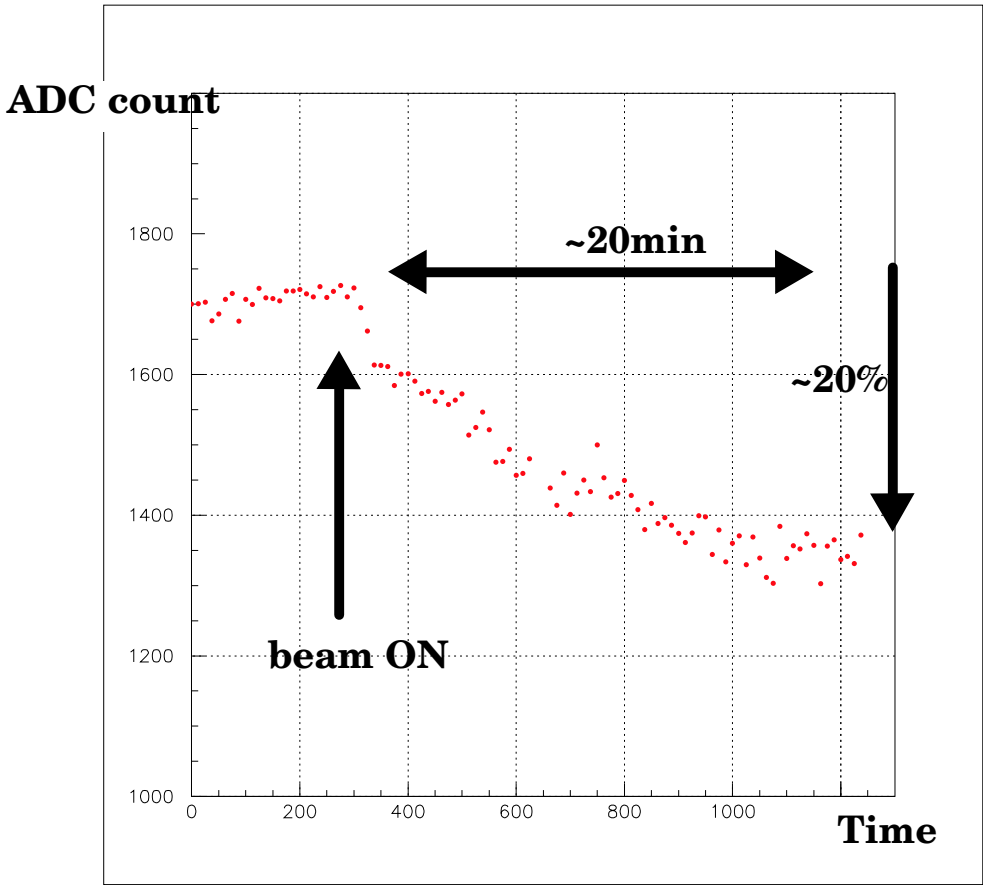

Figure 2.6: Output of a First Version PMT

Since not only gamma rays but also a large amount of neutrons entered the large prototype detector, PMTs inside the detector were exposed to scintillation light from the thermal neutron capture process and the elastic scattering process. It should also be noted that this phenomenon was observed only when PMTs were exposed to liquid xenon, not when they were at room temperature. Therefore, it can be said that the effective quantum efficiency of some first version PMTs dropped due to high rate background events when they were immersed in liquid xenon.

2.2 Background Source in aspects of PMT operation

There are three major backgrounds to PMT operation during $\mu^+ \to e^+\gamma$ search ;

1. Gamma rays from radiative muon decays, $\mu^+ \to e^+\nu_e\overline{\nu}_\mu\gamma$: $\sim 0.4\mu A$ in terms of average anode current
2. Gamma rays from electron-positron annihilation
3. Neutrons produced through the interaction of protons with materials of accelerator elements. : $<\sim 1\mu$[A]

For calibration of liquid Xe calorimeter, gamma rays from π^0 decays ($\pi^0 \to \gamma\gamma$) produced in the charge-exchange reaction ($\pi^- + \mathrm{p} \to \mathrm{n} + \pi^0$) will be used. Neutrons from this charge-exchange reaction enter the liquid xenon calorimeter, which becomes a background to PMT operation. The number of neutrons entering the calorimeter amounts to 20neutrons/cm^2/sec at worst, corresponding to $\sim 2\mu$ [A] in terms of average anode current.[4]
Considering all the backgrounds listed above, the amount of backgrounds entering one PMT is estimated to be 1.0×10^7 photoelectrons per seconds at worst, or 2μ [A] in terms of average anode current of PMT.

2.3 PMT Test at ICEPP, Univ. of Tokyo

A study on stability of the second version and the final version PMT under high rate background environment became urgent task. With PMT Test Facility at ICEPP, Univ. of Tokyo, the low temperature performance of the second and final version PMT was tested. This facility is characterized by its simple and easy operation, which enables the various low temperature performance test on PMT.

2.3.1 ICEPP PMT Test Facility

In order to study the cryogenic performances of PMT, PMT test facility was made at ICEPP, University of Tokyo. This facility consists of xenon storage tank, xenon purifier, and a chamber called Small Xenon Chamber where xenon is liquefied and various tests of PMTs are conducted. (Fig.2.7) The flow diagram of this system is shown in Fig.2.8.
Small xenon Chamber is a cylindrical vessel whose active volume is $\phi 102mm \times 490mm$. At the top of the chamber, a pulse tube refrigerator and liquid-nitrogen cooling pipe are equipped for liquefaction of xenon. Since there is no mechanical moving part in the low-temperature side of the pulse tube refrigerator, noise from the refrigerator into the chamber is minimized and a long-term operation can be easily achieved. We use AISIN PR121 as a pulse tube refrigerator whose cooling power is 25 W at 165K. The temperature of a cold head of the refrigerator is monitored by Platinum thin film resistance (Pt100) and is adjusted to 165K using thermofoil heater equipped in the cold head. The chamber is surrounded with a vacuum insulation layer, reducing static heat load to 3W.
Facing to ^{241}Am alpha source and blue LED located at the center of the chamber, two PMTs are installed inside the chamber(Figs. 2.9 ,and 2.10). Soon after entering liquid xenon, alpha particle deposits its energy of 5.5MeV with a range of 1.343×10^{-2}[g/cm^2],

i.e. approximately 40 μm, which creates scintillation light from liquid xenon. Therefore, this alpha source can be regarded as a point-like light source in liquid xenon.

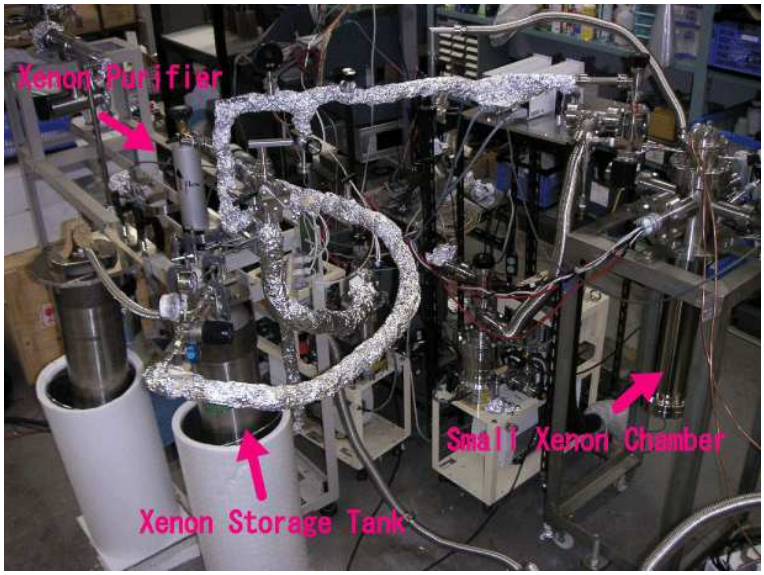

Figure 2.7: ICEPP PMT Test Facility

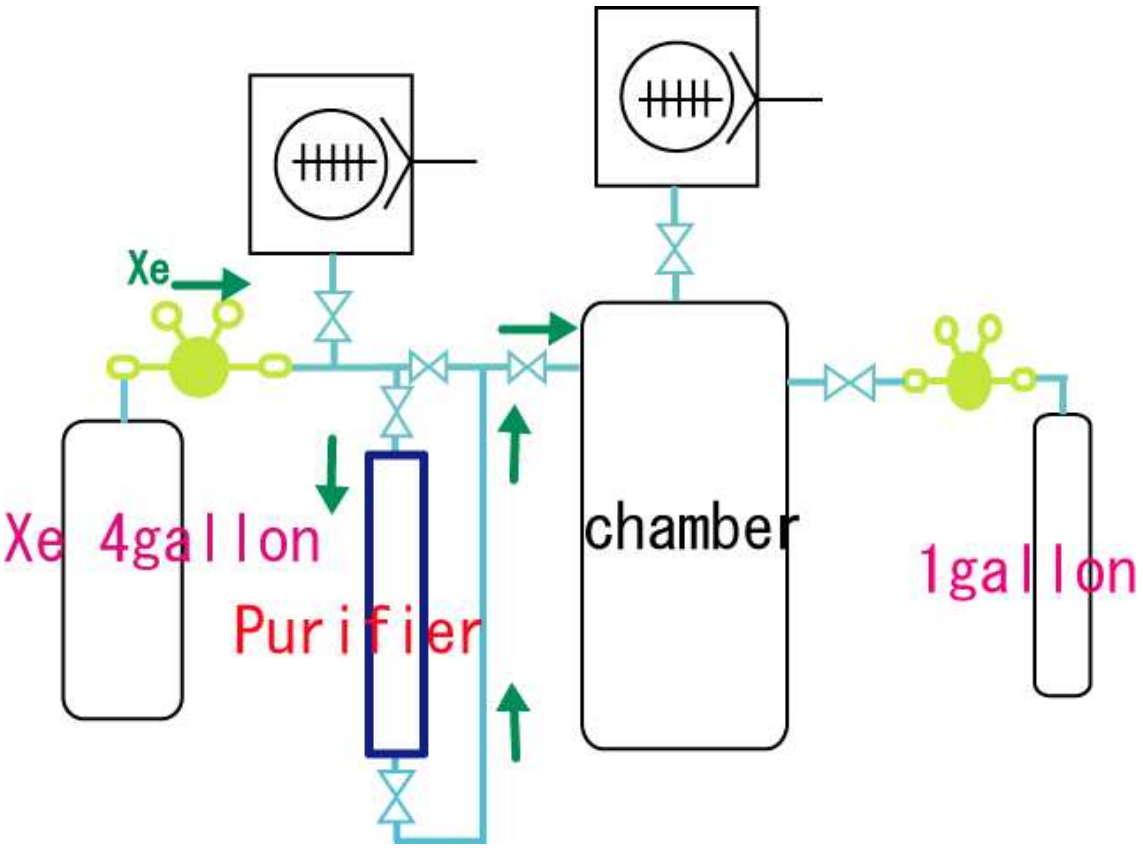

Figure 2.8: Flow diagram of ICEPP PMT Test Facility

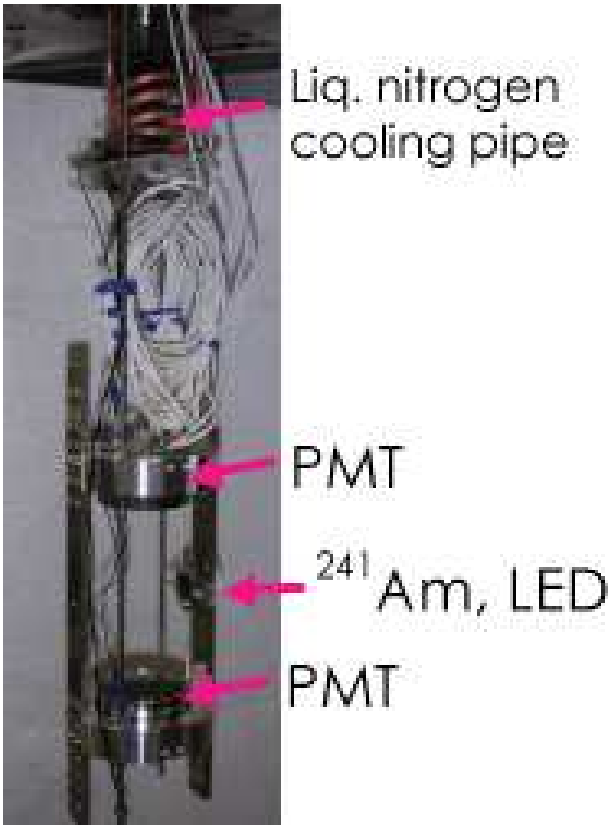

Figure 2.9: Inside Small xenon Chamber

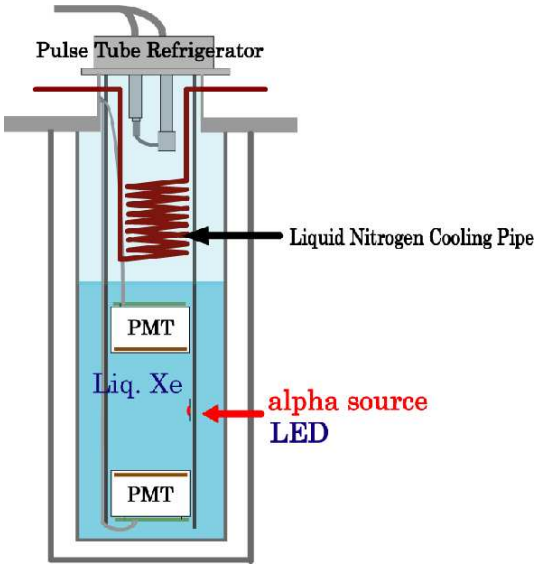

Figure 2.10: Schematic view of Small xenon Chamber

2.3.2 Operation

Small xenon Chamber and gas pipes are initially evacuated down to 10^{-4}Pa before operation. During evacuation, the chamber is baked at rather low temperature of 50°C because of the PMTs inside whose temperature must not be higher than 70°C. After the continuous evacuation for one week, the gas xenon of 0.2MPa is filled into the chamber and cooled down to around 165K using the liquid-nitrogen cooling pipe and refrigerator (pre-cooling). Through the pre-cooling process, temperature of the chamber is brought down sufficiently, cool enough to liquefy xenon. This process takes approximately 2 hours. Passing through a noble gas purifier (Oxisorb), gas xenon is then supplied to the chamber to be liquefied. The gas purifier removes impurities in gas xenon, such as Oxygen and water, to ppb level. Since such impurities cause the absorption of scintillation light from liquid xenon, the water contamination level should be reduced to ppm level. For this reason, baking process and the purification is an integral process for operation.
Liquefaction continues for 2 hours and 2 liters of liquid xenon can be obtained in the chamber. Once xenon is liquefied, it is maintained stably at 168K and 0.10MPa by the refrigerator, whose cold head is monitored and controlled by Pt100 and thermofoil heater, mentioned in the previous section.
PMT tests starts 6 hours after liquefaction finished, waiting for PMTs to be stabilized. Fig.2.11 shows the time dependence of typical PMT output from the α source as a function of the time immediately after the chamber was filled with liquid xenon. As shown in Fig.2.11, PMT output increases for approximately one hour after the liquefaction, and

then gradually decreases. The increase in PMT output is thought to be caused by the contraction of PMT dynodes. When PMT is cooled down, the dynodes of PMT shrink, which shorten the distance between them. This geometrical change is thought to be a cause of the increase in PMT gain, or the increase in PMT output. Meanwhile the decrease in PMT output reflects the temperature of an inside of PMT. As PMT is cooled down slowly, the quantum efficiency gradually decreases, which results in the gradual decrease in PMT output.
PMT output gets stable within $\pm 1\%$ in 6 hours after the liquefaction. Detail of PMT output stability is discussed in 2.3.4.

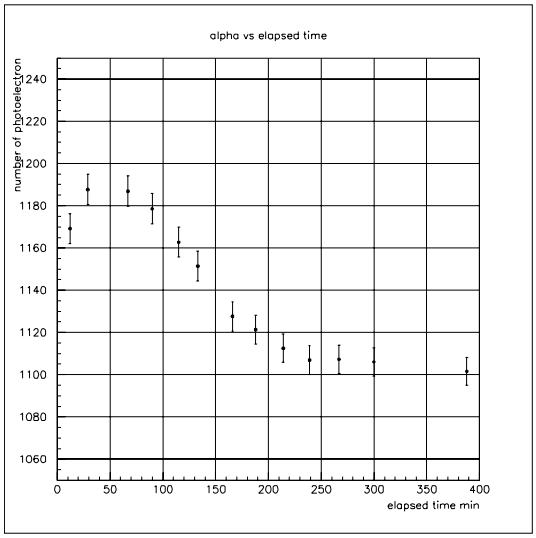

Figure 2.11: Time dependence of PMT Output after liquefaction

2.3.3 PMTs Calibration

PMT gain calibration was done prior to the cryogenic performance test of PMT. By flashing the blue LED at 500Hz with a LED driver at several different intensities, ADC spectrum of PMTs were taken. Assuming negligible fluctuation of LED intensity, the standard deviation of the ADC spectrum (σ) depends on the number of photoelectrons (N_{pe}) observed by the PMT:

$$\sigma^2 = \sigma_0^2 + \frac{\overline{ADC}^2}{N_{pe}} \tag{2.1}$$

where $\overline{ADC}$ is the mean of the ADC spectrum and σ_0 is a standard deviation of pedestal. The variable N_{pe} is expressed in terms of the PMT gain G as:

$$N_{pe} = \frac{\overline{ADC} \times C}{e \times G} \tag{2.2}$$

where C is the least count of the ADC, 0.25pC, and e is the electric charge of an electron. From Eq.2.1 and Eq.2.2, σ^2 can be given by the following equation:

$$\sigma^2 = \sigma_0^2 + \frac{e \times G}{C} \times \overline{ADC} \tag{2.3}$$

As σ^2 is proportional to $\overline{ADC}$, PMT gain can be evaluated from the ratio of σ^2 and $\overline{ADC}$. Fig.2.12 shows a typical ADC spectrum of the PMT outputs in a calibration run and Fig. 2.13 shows an example of the linear relation between σ^2 and $\overline{ADC}$.

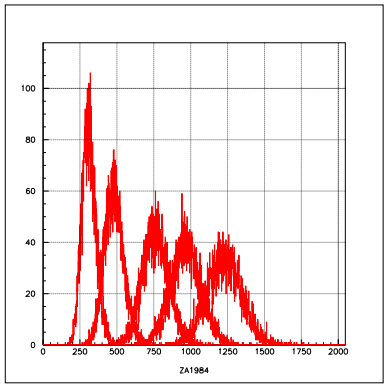

Figure 2.12: Typical ADC Spectrum of gain calibration

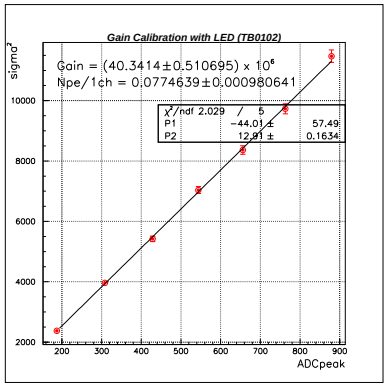

Figure 2.13: Linear relation between variance and mean of ADC

2.3.4 stability of PMT

The stability of PMT was investigated using PMT response to α source events, which was counted by ADC. As described in 2.3.1, this *alpha* source is a point-like constant light source in liquid xenon, so that the stability of PMT can be monitored by observing the α event. ADC mean values of every 2000 events, which corresponds to every 10 seconds, are calculated. 8 PMTs are studied and all of them are found to be stable within ± 1 % (full width). Fig.2.14 shows the time dependence of ADC mean of one PMT. ADC mean values are projected onto a histogram and its variance is evaluated by fitting it with Gaussian. Its stability was found to be ± 0.87 % in full width and 0.3% in sigma.

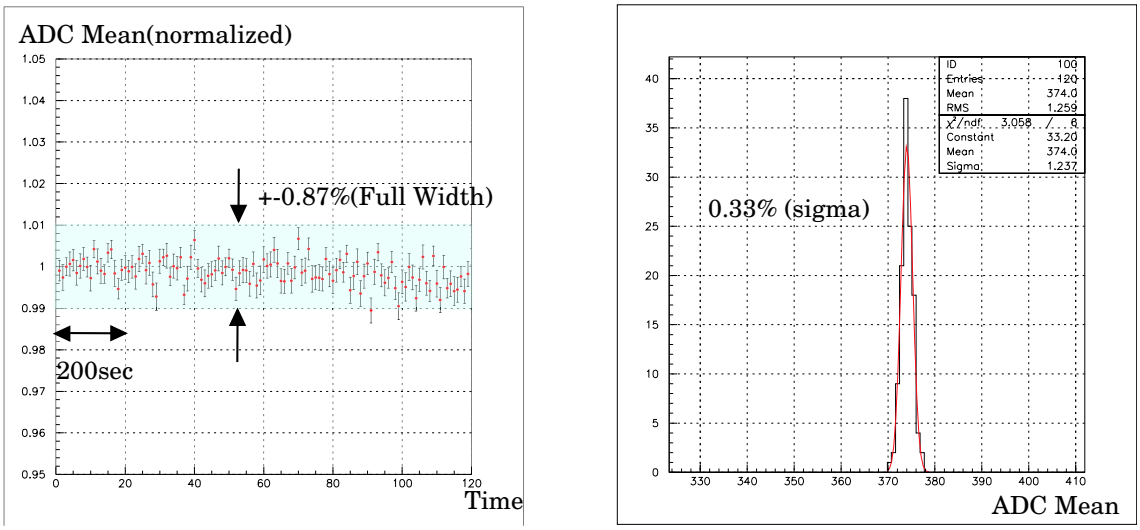

Figure 2.14: Time stability of PMT

2.4 Rate Dependence Test at Liq. Xe

2.4.1 Condition and Procedure

The second and final version PMTs were installed in Small xenon Chamber and measured 5.5MeVα event. At the same time, a blue LED was operated to simulate the high rate background environment. For twenty minutes α events were taken under hight rate background environment, and then, the LED was switched off to take another α events for twenty minutes. Thus, a pair of data sets were obtained, α run under background environment and one under no background, and they were compared. Since this α source is a point-like constant light source in liquid xenon, stability of the PMT under high rate background environment can be monitored by observing α events as described above. PMTs were tested under various background environment by changing the intensity and the rate of the LED. From now on, a blue LED simulating high rate background environment is referred to as "background LED".
We also took data to estimate the photon flux from the background LED. The photon flux is expressed in terms of the photoelectron yield and PMT anode current induced by background LED. The number of photoelectrons (N_{peLED}) can be obtained by the following equation;

$$N_{peLED} = \frac{\overline{ADC_{LED}} \times C}{e \times G} \tag{2.4}$$

Here, $\overline{ADC_{LED}}$ is ADC mean of background LED event, "C" is the least count of the ADC, 0.25pC , and "e" is the electric charge of an electron. "G" refers to PMT gain. The PMT anode current (I_{LED}) can also be calculated;

$$I_{LED} = \overline{ADC_{LED}} \times C \times R_{Hz} \tag{2.5}$$

where R_{Hz} is background LED rate.
The intensity and the rate of background LED was adjusted to $10^6 \sim 10^7$ photoelectrons per seconds, corresponding to $0.1\mu \sim 1\mu$A at 1×10^6 gain.
Alpha events were triggered by α event signals of the PMTs, or self-trigger of an individual PMT, and were vetoed by NIM Clock Generator which generated pulses to trigger background LED. The anode signals of 2 PMTs were digitized by CAMAC ADC connected to a PC. A block diagram of DAQ system is shown in Fig.2.15.

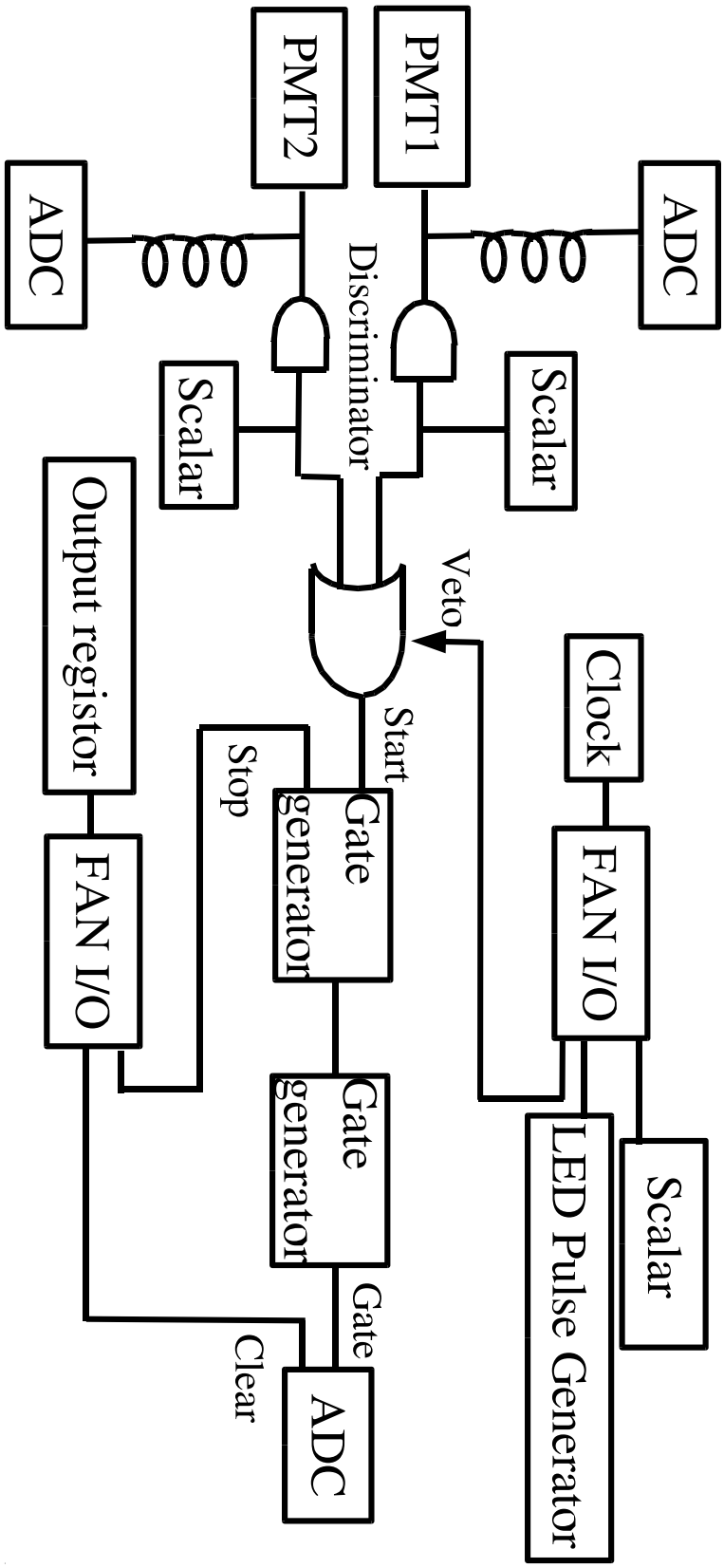

Figure 2.15: Block diagram of DAQ system

2.4.2 Analysis of Rate Dependence of PMT

Deterioration of PMT output under high rate background environment is mainly caused by two reasons. One is an exponential decrease in the effective quantum efficiency of photocathode over several minutes timescale; the phenomenon observed during the beam test at PSI in 2003 (Fig.2.16, Sec. 2.1). The other is a gain variation due to the excessive anode current in PMT base circuit on a timescale of nanosecond or less; Fig. 2.17 shows time dependence of PMT output as a function of time after PMTs were exposed to high rate background environment simulated by a blue LED. A sudden increase in PMT output is observed, which is thought to be caused by the gain variation mentioned above.

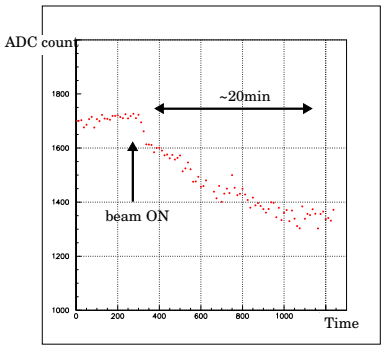

Figure 2.16: Output Deterioration of First Version PMT

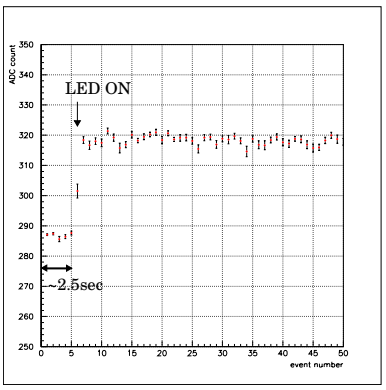

Figure 2.17: PMT Gain shift due to excessive anode current of base circuit

Therefore, the stability of PMT output under high rate background environment needs to be investigated from two different points of view; time dependence of PMT output on few minutes timescale to see photocathode tolerance, and a variation in a mean of ADC spectrum as a function of anode current of PMT induced by background LED to see the gain shift of PMT.

Photocathode tolerance to high rate background

The rate-dependence of PMT photocathode is evaluated by monitoring the stability of PMT output under four different high rate background environment. Here, the stability of a final version PMT is evaluated. The ADC mean values of every 2000 events, corresponding to every 10 seconds, are calculated and are projected onto a histogram. The time dependence of ADC mean values and the variance of the histogram are evaluated. The results are shown in Fig.2.18 and in Fig.2.19.
The time dependence of PMT output over a few seconds timescale is thus evaluated, and the stability within ± 1 % (full width) is confirmed up to 1.0×10^7p.e./sec background. Up to 4.1×10^7p.e./sec background, the stability of PMT is found to be within 0.6% in sigma.

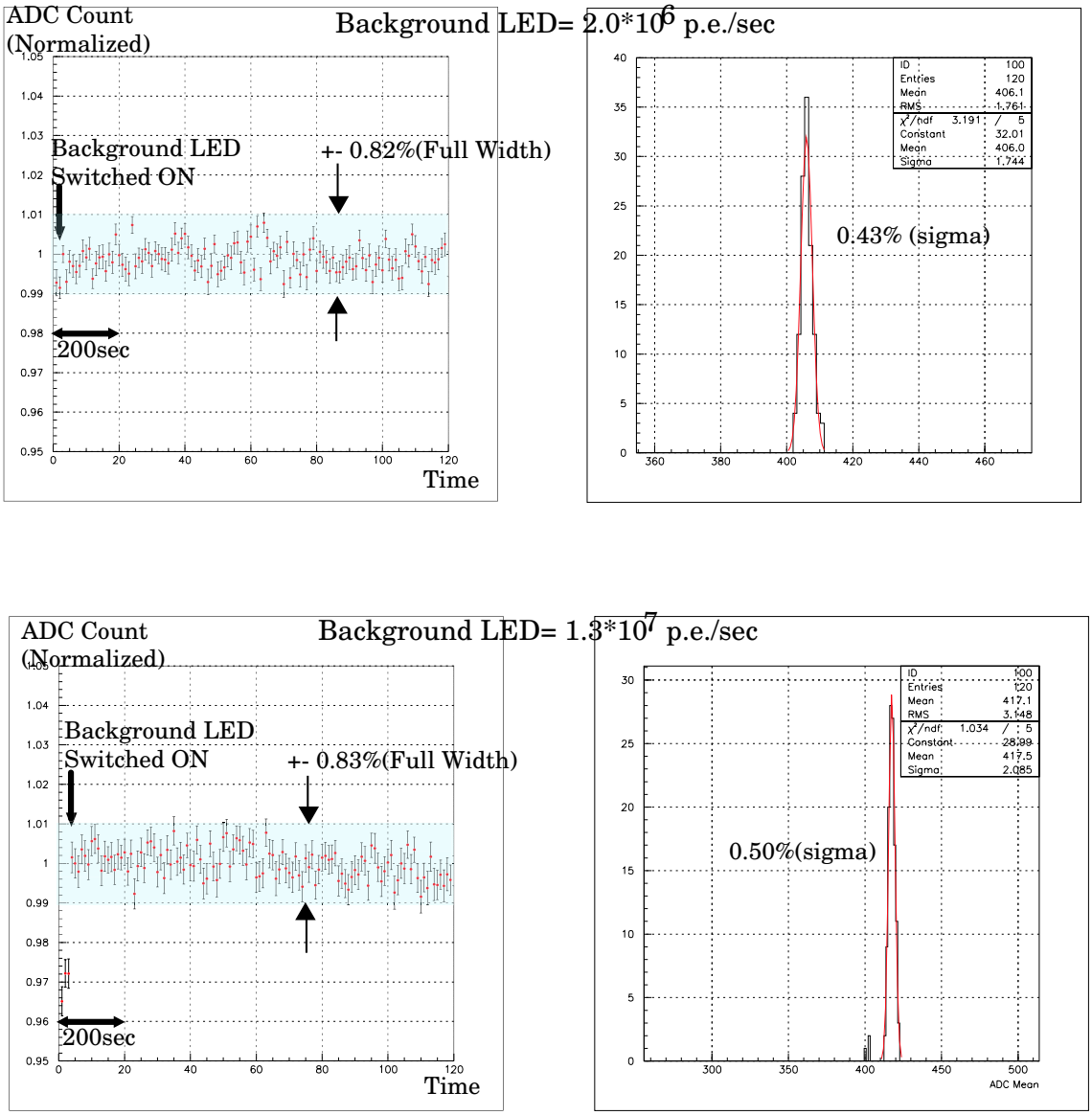

Figure 2.18: Time dependence of a PMT output under background environment

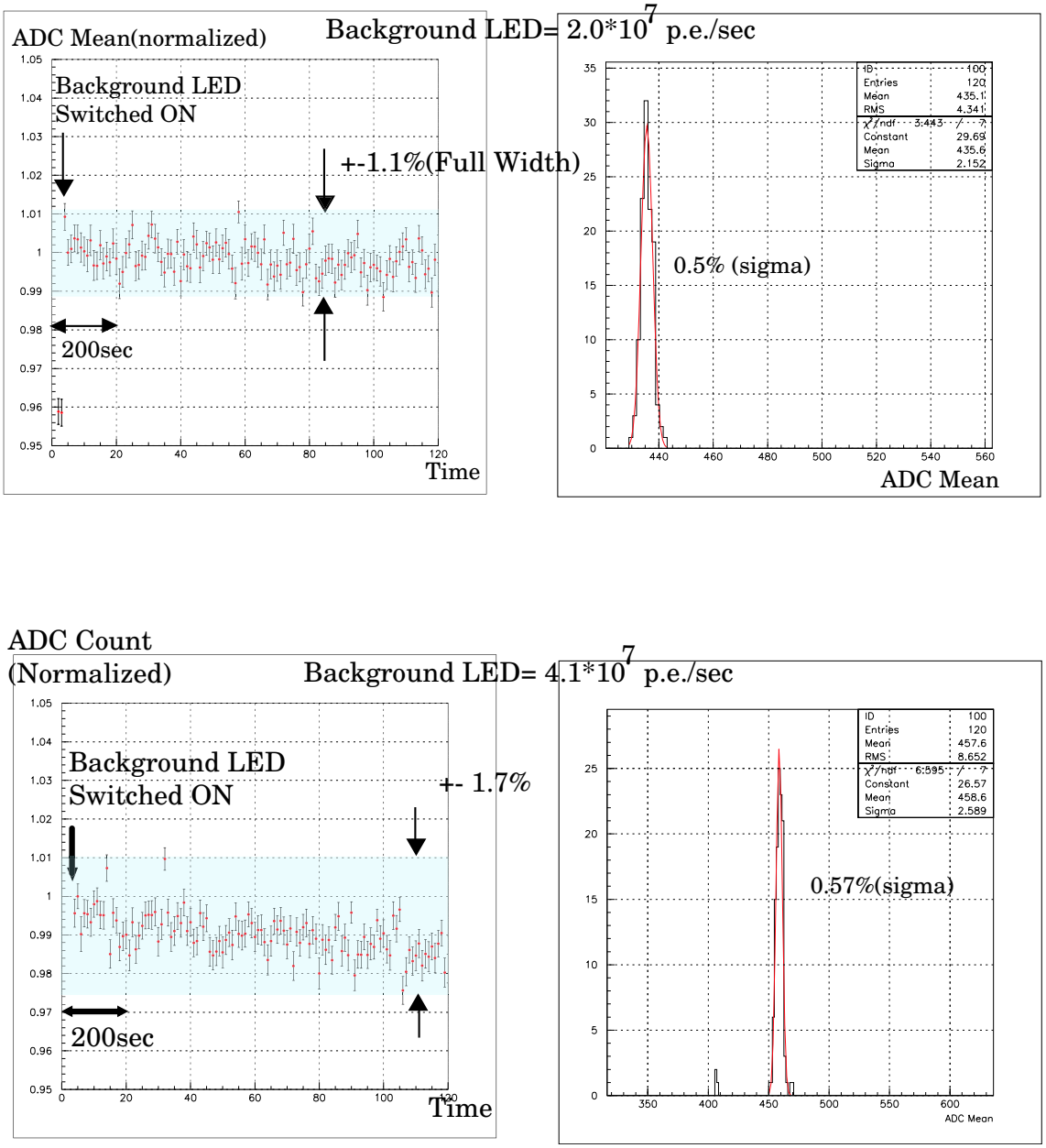

Figure 2.19: Time dependence of a PMT output under background environment

PMT base tolerance to high rate background

The gain shift of PMT is evaluated by comparing α event under background environment and that under no background. ADC mean of α event under background environment is normalized by that under no background, and its dependence on average anode current induced by background LED is studied. Fig. 2.20 shows the result for 6 PMTs. All of them are second version PMTs. We can see that outputs from 5 PMTs begin to shift when their average anode current exceeds 0.5μ [A], which means PMT base tolerance is up to 0.5μ [A]. Meanwhile, we also find that the dependence of a PMT output on its average anode current is different from that of other 5 PMTs. The gain shift of this PMT occurred under rather modest background environment, 0.06μ [A] in terms of average anode current. This can be understood as a defect of a capacitor on the base circuit, or the decrease in its capacity when it is cooled down.

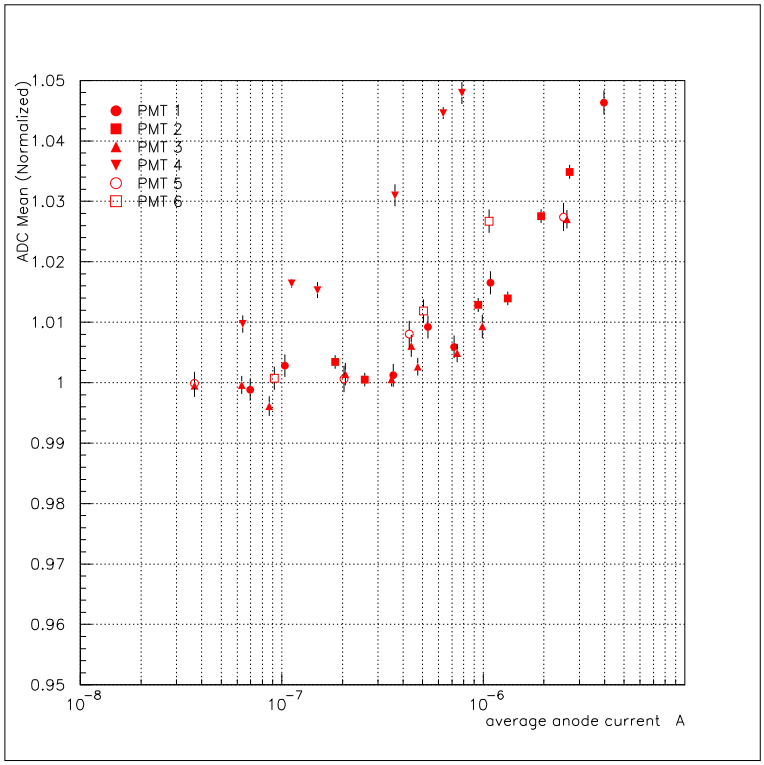

Figure 2.20: A comparison of gain shift as a function of average anode current induced by background LED

The Limit of PMT stability

In MEG experiment, backgrounds to PMT operations are generated by reactions of muons, protons and pions, as described in Sec.2.2. Their amounts can be monitored in several ways, for example, monitoring beam intensities with beam monitors, counting neutrons with neutron counters such as ^3He counters, Bonner Sphere [4], and so on. If the amount of background can thus be evaluated precisely, it will be able to monitor the gain shift of PMT, since the gain shift has a fast response to a background; nano seconds or less. On the other hand, a decrease in effective quantum efficiency of photocathode is difficult to monitor because of its slow response; a few seconds or more. Therefore, the instability of PMT output due to a decrease in effective quantum efficiency of photocathode will have a larger effect to the calorimeter performance rather than that due to a gain shift of PMT. The effect of instability of PMT on calorimeter performance was evaluated by calculating an energy resolution of large prototype detector using its Monte Carlo simulation. The large prototype detector is briefly explained in Sec.2.1. In the Monte Carlo simulation, 52.8 MeV γ rays were irradiated at the center of large prototype detector, and photoelectron yield from all PMTs $N_{p.e.}$ was calculated. With this information, the energy resolution for 52.8 MeV γ under high rate background environment was evaluated as below.
In general, the energy resolution is a function of the energy deposited in the detector, or a total photoelectron yield from PMTs which follow Poisson statistics. The energy resolution can be expressed as;

$$Resolution = \frac{\Delta E}{E} = \frac{\sigma}{Mean} = \frac{\sqrt{N_{p.e.}}}{N_{p.e.}} = \frac{1}{\sqrt{N_{p.e.}}} \tag{2.6}$$

where $N_{p.e.}$ is a total photoelectron yield, and from the simulation, it is $N_{p.e.} = 1.54 \times 10^5$ [photoelectrons]. Therefore, the optimum energy resolution for 52.8 MeV γ is $\frac{1}{\sqrt{1.54\times10^5}} = 0.0026$, that is 0.26%.
In addition to the fluctuation in the number of photoelectrons ($\sigma_{p.e.}$), a number of external factors can affect the overall resolution of a detector. Here, for simplicity, only fluctuation in a PMT output due to a decrease in quantum efficiency of photocathode is considered (σ_{BG}). In large prototype detector, 228 PMTs are installed, so that the fluctuation in 228 PMTs output will be $\sigma^2_{BGtotal} = 228 \times \sigma^2_{BG}$, assuming that all PMTs are exposed to the same amount of background. Consequently, the width of energy spectrum of the detector can be written as follows;

$$\Delta E^2 = \sigma^2_{p.e.} + \sigma_{BG}all^2 = \sigma^2_{p.e.} + 228 \times \sigma^2_{BG} \tag{2.7}$$

Therefore, the energy resolution of large prototype detector will be expressed as;

$$\frac{\Delta E}{E} = \frac{\sqrt{\sigma^2_{p.e.} + \sigma^2_{BGtotal}}}{Mean} = \frac{\sqrt{N_{p.e.} + 228 \times \sigma^2_{BG}}}{N_{p.e.}} \tag{2.8}$$

If we impose a rather severe requirement, 0.3%, upon this energy resolution, the fluctuation in a PMT output must be limited to 2.4%;

$$\frac{\Delta E}{E} < 0.003 \tag{2.9}$$

$$\frac{\sigma_{BG}}{N_{p.e.}/228} < 0.024 \tag{2.10}$$

Here, all the PMTs are supposed to yield the same photoelectrons from 52.8MeV γ events. In Sec.2.4.2, we saw that photocathode tolerance of final version PMT to high rate background up to 4.1×10^7p.e./sec was investigated and the fluctuation in PMT output was found to be within 0.6% (sigma). Consequently, it can be said that the stability of final version PMT adequate for the operation of the calorimeter under high rate background.

2.5 PMT Test Using The Second Version Base Circuit

The gain shift of PMT can be suppressed in two ways;

1. Redesign of the base circuit
2. Placing neutron shields around the calorimeter

The latter is not so easy since there won't be much space around the calorimeter. Therefore, the base circuit was redesigned, and its performance was tested using the PMT Test Facility.

2.5.1 Basic Idea for the Redesign of PMT Base

The gain shift of PMT is thought to be caused by changes in voltage distribution across the last few dynode stages due to excessive average anode current. Fig.2.21 is a simplified model showing photomultiplier operation with two stages of dynodes and three resistors, R1 to R3.

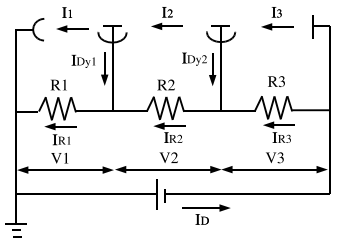

Figure 2.21: Basic operation of photomultiplier and its base circuit without light input

When light is not incident on a photocathode, the relation between current and voltage of components in base circuit is given as;

- Interelectrode current: $I_1 = I_2 = I_3 = 0$[A]
- Electrode current : $I_{Dy1} = I_{Dy2} = 0$[A]
- Base circuit current : $I_{R1} = I_{R2} = I_{R3} = I_d$
- Interstage voltage : $V_n = R_n \times I_n$

While light is striking the photocathode, the interstage voltage is changed by the induced current which flows through the photomultiplier and its base (Fig:2.22).

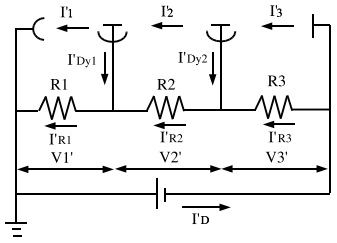

Figure 2.22: Basic operation of photomultiplier and its base circuit with light input

The current flowing through the dividing resistors, R1 to R3, can be written as follows;

$$I'_{R3} = I'_d - I'_3 \tag{2.11}$$
$$I'_{R2} = I'_d - I'_3 + I'_{Dy2} \tag{2.12}$$
$$I'_{R1} = I'_d - I'_3 + I'_{Dy2} + I'_{Dy1} \tag{2.13}$$

Therefore, the interelectrode current has the following relation;

$$I'_1 < I'_2 < I'_3 \tag{2.14}$$

Thus, the interstage voltage, Vn, becomes smaller at the latter stages;

$$V'_1 > V'_2 > V'_3 \tag{2.15}$$

The interstage voltage of last two dynodes, V_3, is only required to collect the secondary electrons emitted from the last dynode to anode, so that it has little effect on the anode current even if it drops. While the increases in V_1 and V_2 raise the secondary emission and boost the overall gain. Thus the gain shift of PMT output occurs.
There are several specific methods to cope with this nonlinearity [5];

1. Increasing the base current
   Simple solution for this problem will be just increasing the current, I'_d, so as to minimize the changes in the interstage voltage distribution. However, this method accompanies heat emanating from the base circuit.

2. Using Zener Diode (Fig. 2.23)
   The gain shift of PMT output can be suppressed by placing Zener diodes on the last few dynodes because it serves to maintain the interstage voltage constant.

3. Using the active voltage divider circuit (Fig.2.24)
   By mounting transistors in place of the dividing resistors in last few stages, the interstage voltage is stabilized since it is not affected by the interelectrode current inside PMT.

4. Booster method (Fig. 2.25)
   The interstage voltage is maintained constant by supplying voltages directly to the last few stages.

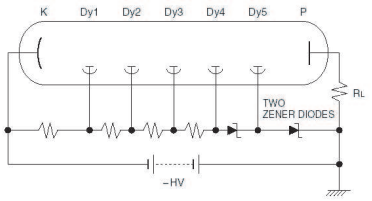

Figure 2.23: Voltage Divider Circuit using Zener Diode [5]

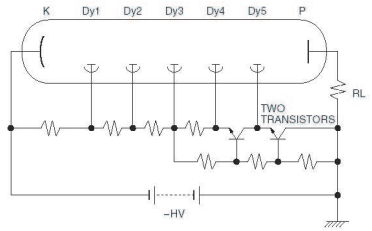

Figure 2.24: Active Voltage Divider Circuit [5]

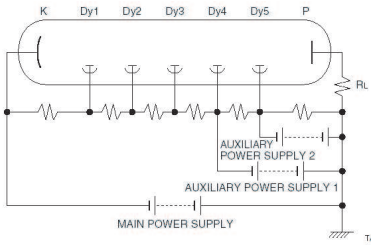

Figure 2.25: Booster Method [5]

Since our PMTs are operated in the liquid xenon, the heat load from their base circuit must be minimized. And in addition, less cables and less electric parts is desirable since our calorimeter should be compact. From this point of view, a base circuit using Zener diodes was investigated as the second version PMT base circuit.

2.5.2 Zener Diode and Second Version Base Circuit

Zener diode is a semiconductor commonly used as a voltage regulator. It uses a p-n junction in reverse bias to make use of the Zener effect, which is a breakdown phenomenon in a nondestructive manner. Applying sufficient reverse voltage, the p-n junction will experience a rapid avalanche breakdown and it conduct current in reverse direction. (2.26) Under this condition, the voltage across the diode is nearly independent of the current.

For PMT base circuit, a low noise Zener diode, RD-S series manufactured by NEC Co., is adopted. The current-voltage characteristics of the NEC RD-S series Zener diode was measured in room temperature. Fig.2.27 shows the result.

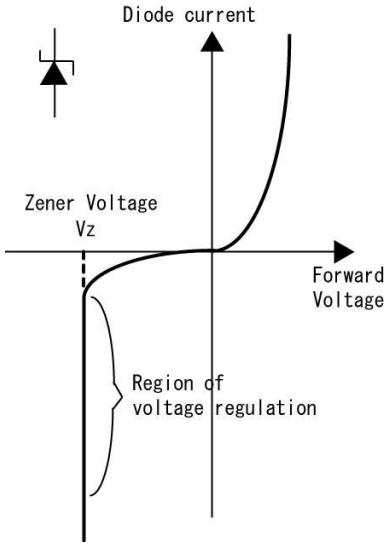

Figure 2.26: Current-Voltage characteristics of Zener diode

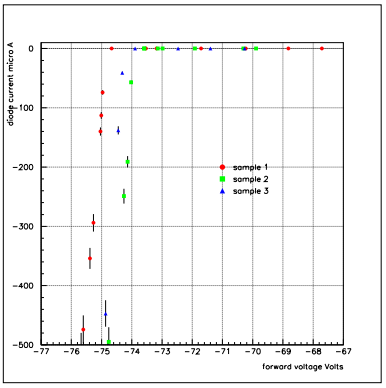

Figure 2.27: Current-Voltage characteristics of NEC RD-75S Zener diode

The current-voltage characteristics in liquid nitrogen temperature was also measured by immersing Zener diode in liquid nitrogen. The results are summarized below. Zener voltages decrease as diodes are cooled down, and this decrease can be explained by temperature coefficients of Zener diodes.

Type	Temperature Coefficient [6]	Zener Voltage at 25°C(298K)	Zener Voltage Zener Voltage in liquid nitrogen (70K)
RD82S	85mV/°C	77.0 - 87.0	57.6 - 67.6
RD75S	75mV/°C	70.0 - 79.0	52.9 - 61.9
RD68S	70mV/°C	64.0 - 72.0	48.0 - 56.0
RD62S	60mV/°C	58.0 - 66.0	44.3 - 52.3

Zener voltage at liquid xenon temperature can be calculated by considering the temperature coefficient of Zener diode.

Type	Zener Voltage at liquid xenon [V]
RD82S	65.7 - 75.7
RD75S	60.0 - 69.0
RD68S	54.7 - 62.7
RD62S	50.0 - 58.0

Fig. 2.28 shows PMT base circuit with Zener diodes. We call this circuit "the second version base". Precaution should be taken when using this type of base circuit; if the high voltage supplied to PMT is greatly varied, the voltage distribution will be unbalanced compared to other interstage voltages, thus limiting the adjustable range of high voltage. In our base circuit, optimal high voltage is limited to $800 \sim 900$[V] and Zener diodes are selected accordingly.

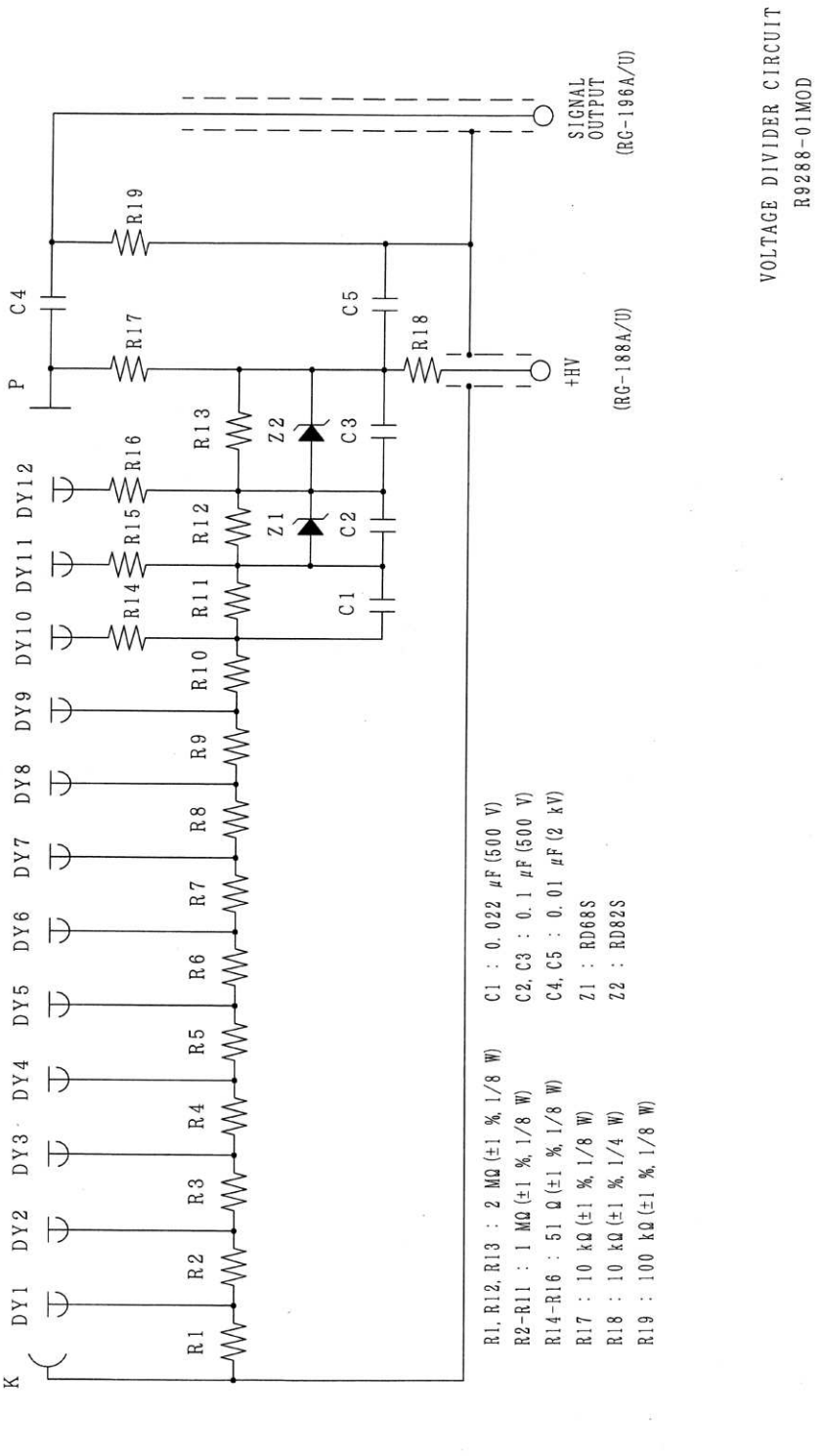

Figure 2.28: The Second Version PMT Base

2.5.3 Rate dependence Test at Liq. xenon

The cryogenic performances of Zener diode and PMT using the second version base circuit was tested in Small Xe Chamber.

Setup

Two PMTs were installed in Small Xe Chamber; one PMT was the second version PMT and was used as a reference. Zener diode was not used in its base circuit. The other PMT was the final version PMT where the second version base was attached. At the center of Small Xe Chamber, ^{241}Am alpha source and a blue LED were located at the distance of 55mm in front of each PMT. (Fig.2.29) The anode signals of 2 PMTs were digitized by CAMAC ADC connected to a PC.

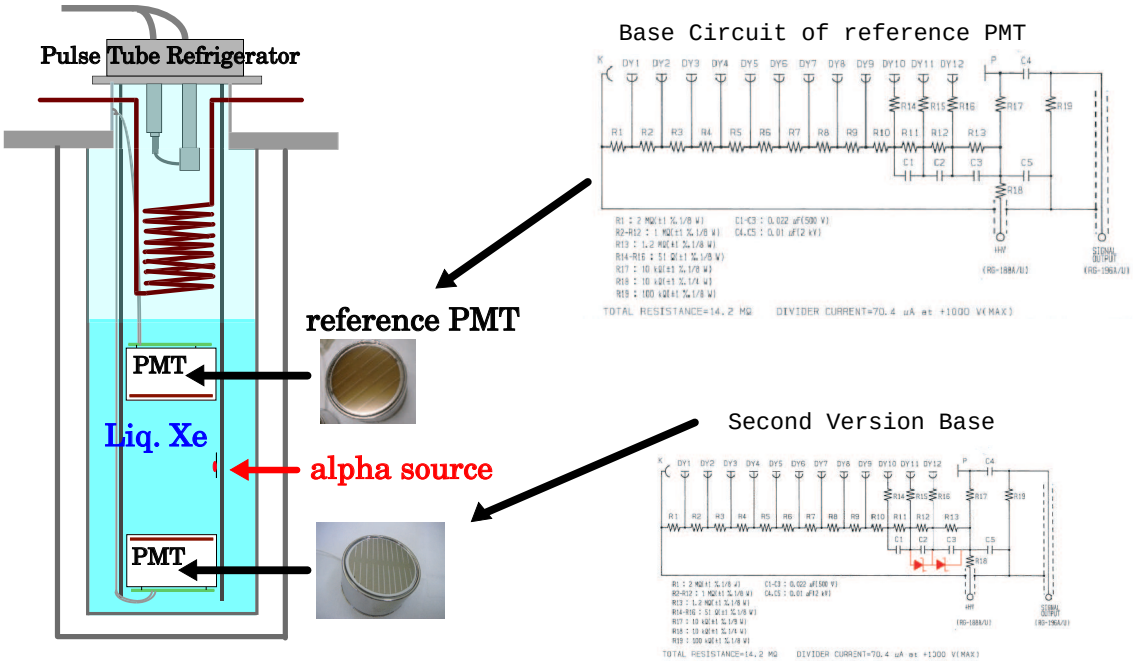

Figure 2.29: Inside Small Xe Chamber

Rate-dependence

The rate dependence of a PMT using second version base circuit is evaluated in the same way discussed in Sec.2.4.2. Fig.2.30 shows the result; PMT with a second version base is found to be stable within $\pm 1\%$ up to 5μ[A].

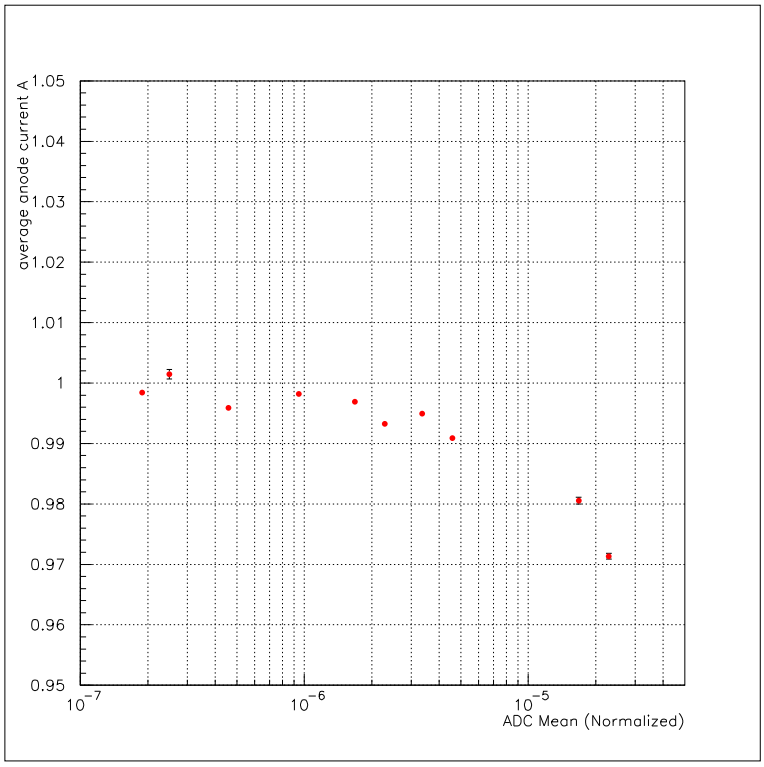

Figure 2.30: The stability of PMT with Zener Diode in its base as a function of average anode current induced by background LED

2.5.4 The noise of Zener diode and its effects

In order to stabilize the gain of PMT, we thus mounted Zener diodes between the last few dynodes and found that this works well in terms of stability. However, there is a relatively large amount of random noise on the voltage across the diode, and it is concerned that this noise affects PMT output.
A Zener diode, NEC RD68S, was soaked in liquid xenon, and its noise was measured using oscilloscope. Fig.2.31 is the circuit used for this measurement and Fig.2.32 shows the outputs on the oscilloscope.

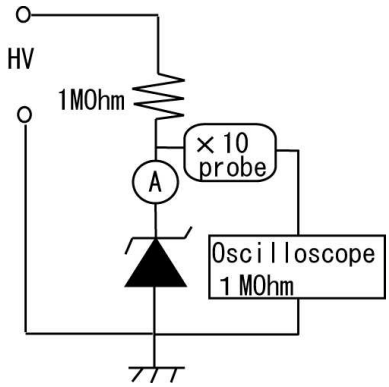

Figure 2.31: A circuit for the measurement of Zener diode noise

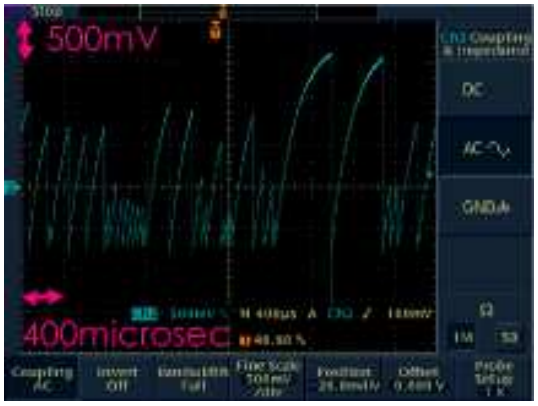

Figure 2.32: Noise of Zener Diode

As shown in Fig.2.32, a sharp drop in voltage across the diode is observed, which, in fact, causes a random noise on PMT output. In order to see the noise level, a PMT with a second version base circuit was placed in liquid xenon, and its output was measured using an oscilloscope. Several waveforms were taken by changing the high voltage supplied to the PMT. As shown in Fig. 2.33, we can see that noise suddenly appeared when voltage supplied to the PMT reached approximately 460[V], which corresponds to the voltage across Zener diode of 57.5[V], just Zener voltage in liquid xenon temperature. The rate of this noise was measured using NIM Scalar, and was found to be a few hundreds [Hz].

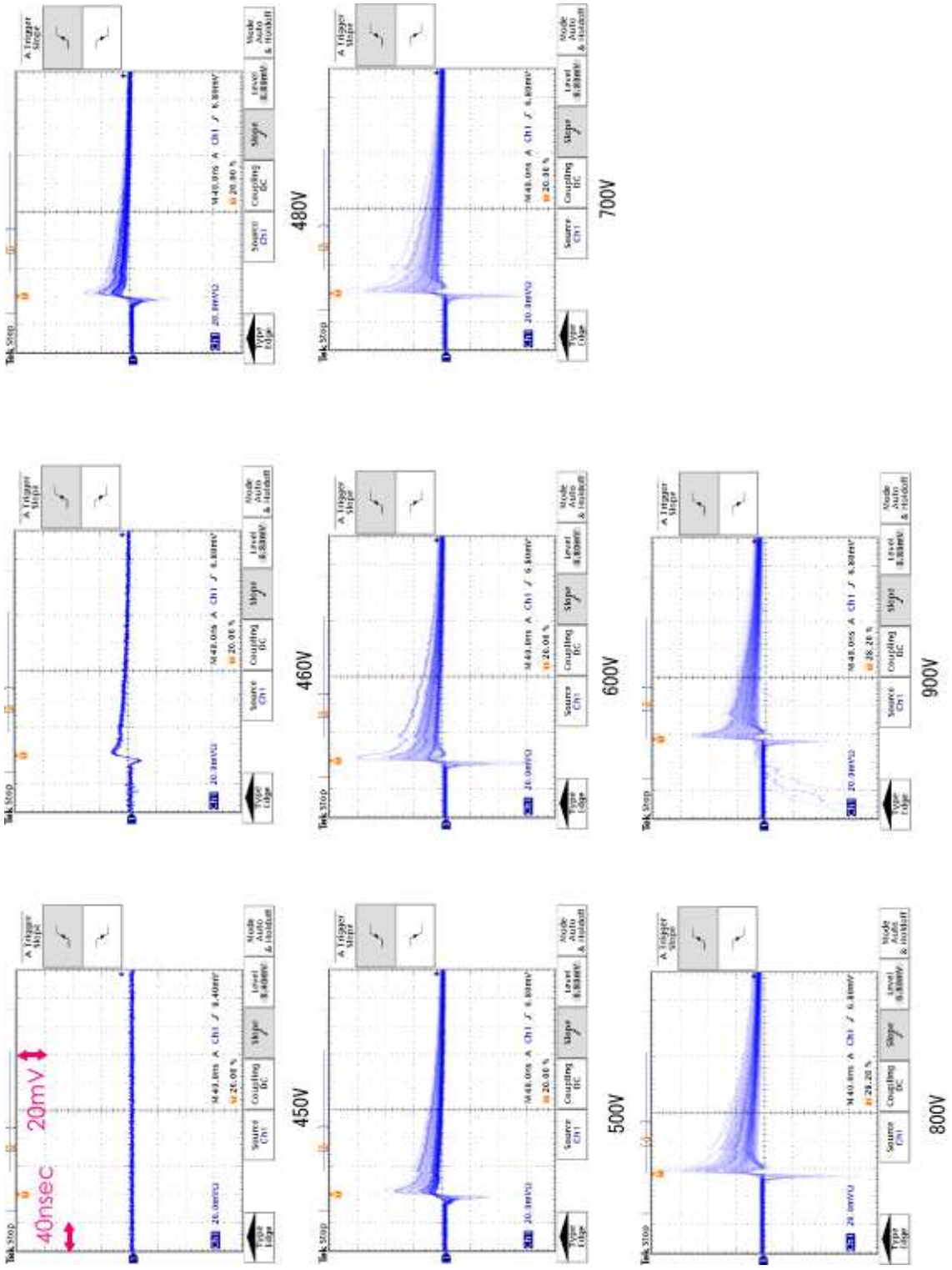

Figure 2.33: Noise on PMT output induced by Zener diode

2.5.5 Effect of noise of Zener diode on Liquid xenon Calorimeter

The noise from Zener diode thus affect the PMT signal, so that it was concerned that this noise might deteriorate the resolution of Liquid xenon calorimeter. Using Monte Carlo Simulation, the effect of the noise from Zener diode on Liquid xenon calorimeter was roughly estimated.
First, 800 Volts were applied to 2 PMTs and their pedestal data were taken. One PMT was the second version PMT and was used for reference. Zener diode was not used in its base circuit. The other PMT was the final version PMT where second version base was attached. Random and no-bias triggers were generated using NIM Clock Generator, and 1000,000 events of pedestal data were taken. The pedestal distribution for 2 PMTs is shown in Fig.2.34. The blue line shows the pedestal distribution of reference PMT, and the red line shows that of PMT whose base circuit contains Zener diode.

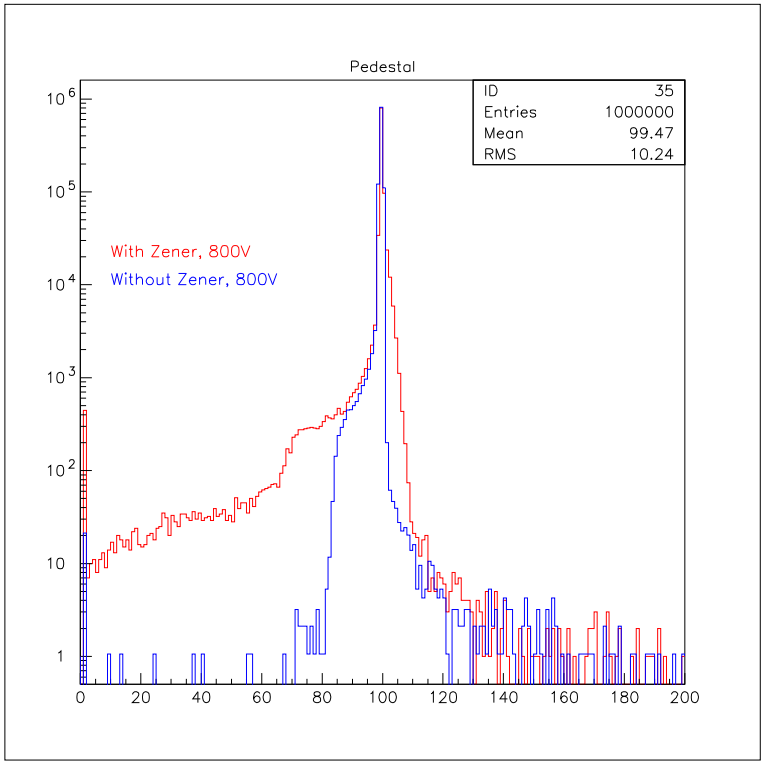

Figure 2.34: Pedestal distribution

In the MC simulation, 52.8 MeV monochromatic gamma rays were irradiated at the center of the large prototype detector, and 30,000 gamma events were generated. The pedestal data of 2 PMTs were merged into this gamma events generated by MC. They are used to give an additional fluctuation to energy spectrum of the gamma events. The result is shown in Fig.2.35. ADC distribution of gamma rays events where effect of Zener diode noise is considered are plotted in red, and gamma rays events where effect of Zener diode noise is not merged are plotted in blue. We can see that there is little difference between them and it can be said that the noise from Zener diode will not affect the resolution of calorimeter seriously. However, a careful study on this noise is needed. For instance, with

waveform analysis, it is able to discriminate the noise from signals of γ events, since the waveform of noise from Zener diode is bipolar, which is quite different from that of signal from γ events.

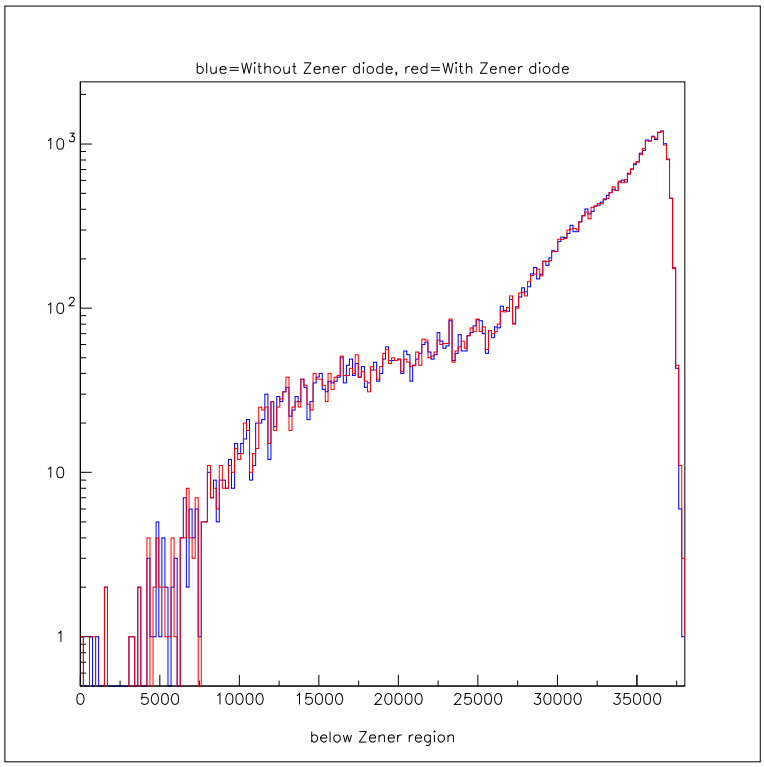

Figure 2.35: Effects of noise of Zener diode on 52.8MeV gamma events

Chapter 3

Filler Study for PMT

In MEG experiment, liquid xenon calorimeter must detect γ rays with extremely high precision. In addition, the experiment aims to detect a rare decay, requiring high detection efficiency of gamma rays. Hence the incident face of the calorimeter where gamma rays pass needs to be designed to minimize the lost of their kinetic energy. In other words, the radiation length of the incident face must be as long as possible.
At the incident face of large prototype detector (Sec.2.1), as shown in Fig.3.1 and Tab.3.1, some organics and minimum amount of metals are used to suppress interactions of gamma rays as low as possible. Though most of the front face of the detector is filled in with materials listed in Tab.3.1, the space between PMT and PMT cover, the part surrounded by a red line shown in Fig.3.1, is left unfilled. When the detector is filled with liquid xenon, xenon seeps into this space, where interaction rate of gamma rays can be increased very much due to the short radiation length of liquid xenon. Therefore, filling the space will improve the efficiency of the calorimeter, so that the way of filling the space and material for a filler has been studied.

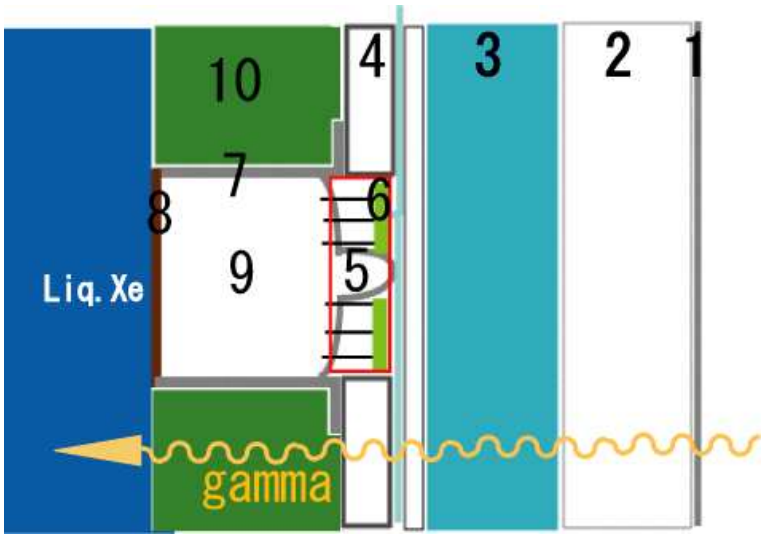

Figure 3.1: The front face of large prototype detector

Table 3.1: Thickness and Material of the front face

No.	Name	Materials	Thickness	Thickness in radiation length
1	Incident Window	Aluminum	0.1mm	0.001
2	Vacuum insulation layer	vacuum	0.0mm	0.0
3	Honeycomb	SUS314	20mm	0.039
4	PMT Cover	Acrylic	16mm	0.046
5	PMT Tip Tube	Pyrex Glass	0.916mm	0.074
6	PCB	G10	2mm	0.011
7	PMT Tube	SUS304	30mm	1.714
8	PMT Window	Synthetic Quartz	3mm	0.024
9	Metal Channel Dynode	SUS+α	0.1512mm	0.086
10	PMT holder	G10	29mm	0,157

3.1 Basic Idea for Filler

The space between PMT and the detector wall is odd-shaped because of PMT Tip and electric parts on base circuit (Fig.3.2 and Fig.3.3). Therefore, the first idea of filling this irregular space was to attach a low-viscosity adhesive directly to a rear of PMT so as to fill the space in tight clearance as shown in Fig.3.4.

Figure 3.2: The rear of PMT

Figure 3.3: The rear of PMT; here, base circuit is removed

Figure 3.4: Filler is attached to the rear of PMT

Since this adhesive will be located at the front face of the liquid xenon calorimeter, it must meet many requirements;

- It must not contaminate liquid xenon.
- It must have long radiation length since incident γ rays pass through a filler.
- It must have the similar thermal expansion characteristics to Kovar glass, of which the rear of PMT is made, since it is cooled down to 165K together with a PMT.

From the requirements above, we selected a mixture of STYCAST and quartz glass as a filler.
STYCAST is a two-component epoxy resin adhesive frequently used for vacuum feed-through. Since it is a low-outgas adhesive, it won't contaminate liquid xenon. Its low viscosity enables to fill the irregular space in tight clearance. In order to minimize the difference in thermal expansion characteristics between STYCAST and Kovar glass, quartz glass beads are mixed with a ratio of 1:1 by weight. The radiation length of the mixture, $x_{0filler}$, is 192.6mm, which is acceptable considering the thickness of a filler to be approximately 11mm.
The radiation length (x_0) of a filler can be simply computed by applying Bragg's rule;

$$\frac{1}{x_{0filler}} = \frac{w_1}{x_{0STYCAST}} + \frac{w_2}{x_{0quartz}} \tag{3.1}$$

where w_1 and w_2 are the fractions by weight of each element in the mixture, $x_{0STYCAST}$ and $x_{0quartz}$ are the radiation length of STYCAST and quartz glass. Substituting $x_{0STYCAST} = 443.7mm$, $x_{0quartz} = 123mm$ and $w_1 = w_2 = 1/2$, one obtains $x_{0filler} = 192.6mm$.

3.1.1 thermal expansion measurement

When a material is cooled down, the average amplitude of atoms' vibration within the material decreases, causing the object to contract. The change in the object's length ΔL can be calculated by a simple equation using the temperature change, ΔT, and the linear expansion coefficient α;

$$\Delta L = \alpha L_i \Delta T \tag{3.2}$$

where L_i is the initial length of the object before it is cooled down. The linear expansion coefficient, α, is specific to the material. The linear expansion coefficient of STYCAST and a mixture of STYCAST and quartz glass were measured. The measurement was done with three materials; one was STYCAST, another was a mixture of STYCAST and quartz glass whose mix ratio was 1:1 by weight, and the other was a mixture of STYCAST and quartz glass whose mix ratio was 2:3 by weight. The procedure of the measurement was as follows.

1. Blocks of the materials were prepared. They were milled into rectangular solid.
2. The length of sides were measured with a caliper at room temperature.
3. The blocks were immersed in liquid Nitrogen and were cooled down to 70K.
4. The length of sides were measured as soon as the blocks were taken out from liquid Nitrogen.
5. From changes in the length of sides before and after the cooling, the linear expansion coefficients were calculated.

Results are summarized in Table 3.2, 3.3 and 3.4.

1. STYCAST

Table 3.2: The result of linear expansion coefficient of STYCAST

Temperature([K])	length of side [mm]
298.7	84.2
76.1	83.4
linear expansion coefficient α	4.3×10^{-5}

2. STYCAST : glass = 1:1 by weight

Table 3.3: The result of linear expansion coefficient of the mixture, STYCAST:quartz=1:1

Temperature([K])	length of side [mm]
299.2	88.75
76.1	88.2
linear expansion coefficient α	2.8×10^{-5}

3. STYCAST:glass = 2:3 by weight

Table 3.4: The result of linear expansion coefficient of the mixture, STYCAST:quartz=2:3

Temperature([K])	length of side [mm]
299.2	87.2
76.1	86.8
linear expansion coefficient α	2.1×10^{-5}

The thermal expansion coefficient of Kovar glass, which covers the PMT rear, is known to be approximately 5×10^{-6}[/K]. From the results listed above, it can be said that the difference in thermal expansion coefficient of Kovar glass and a filler is minimized by mixing quartz glass into STYCAST. The more quartz glass is added to STYCAST, the more the difference in thermal expansion coefficient is minimized. However, the radiation length of filler will be shortened if excessive quartz glass is added into STYCAST. Therefore, we concluded that the optimal compounding ratio of STYCAST and quartz glass is 1:1 by weight.

3.2 Cooling Test of PMT with a filler being attached

A mixture of STYCAST and quartz glass was thus adopted as a filler, and next we started to investigate the way of attaching the filler to the rear of PMT. On working on R&D of a filler, we used PMT samples which rolled off the production line of Hamamatsu Photonics Co.

Our first idea was to use a mold as shown in Fig.3.5. Setting PMT to the mold (3.6), we turned a filler into it and left untouched until a filler hardened. A filler is thus attached to the rear of PMT, as shown in Fig. 3.7.

Though the efforts were made to minimize the difference in thermal expansion characteristics between the filler and the rear of PMT, as described in Sec. 3.1, their linear expansion coefficients are still not the same (Sec.3.1.1), which might cause damage to PMT. Therefore, a cooling test of PMTs with a filler down to 165K was performed for confirmation.

The experimental apparatus is shown in Fig.3.8 and Fig.3.9. The PMTs were placed on a copper stage where a copper cold finger was screwed. This copper cold finger was immersed in liquid nitrogen. Through this cold finger the copper stage and the PMTs were cooled down. The temperature of PMTs was monitored with a Platinum thin film resistance (Pt100) attached to the PMTs and the copper stage, and it was controlled by a heater wound around the copper cold finger. The model of this apparatus is the one used in the measurement of the property of cooled lead molybdate. [7]

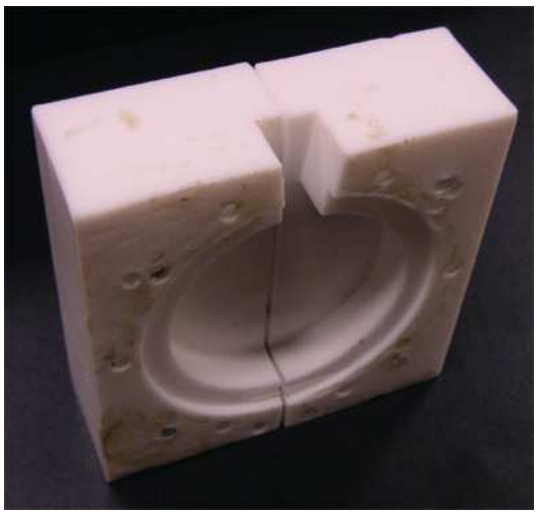

Figure 3.5: The mold for attaching a filler to a rear of PMT

Figure 3.6: a PMT is set to the mold

Figure 3.7: A filler is attached to the rear of PMT using the mold

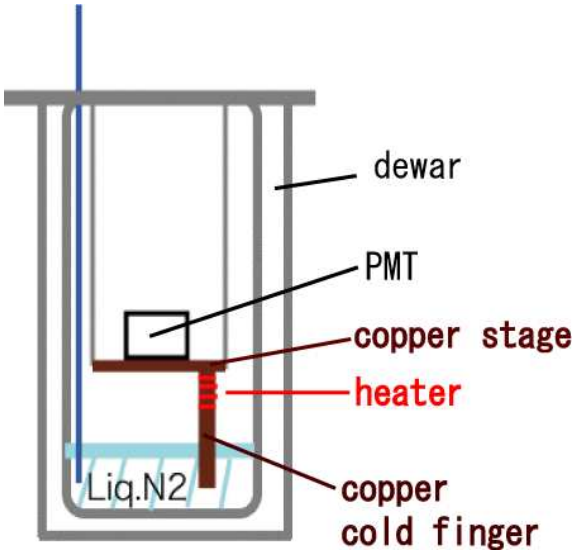

Figure 3.8: The experimental apparatus of the cooling test

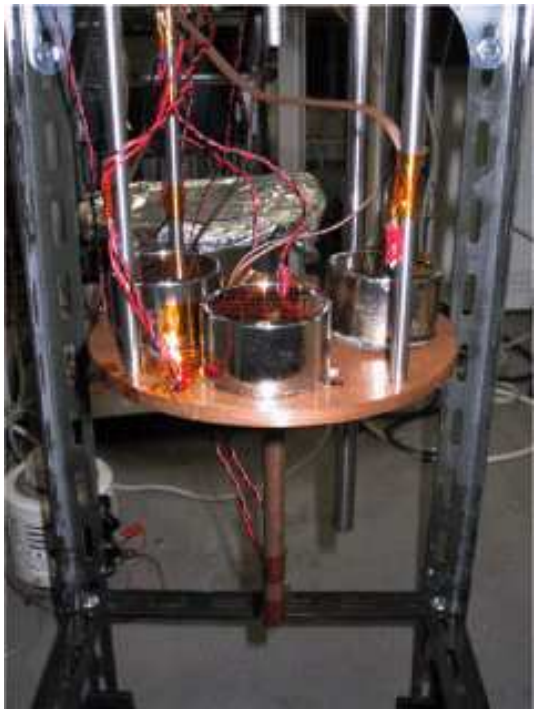

Figure 3.9: The experimental apparatus of the cooling test

The PMTs were taken out of the apparatus after the cooling test, and it was found that photocathodes of all PMTs were discolored, which meant that they were oxidized in air. The PMTs were then carefully taken apart to investigate the cause of the oxidization of the photocathode. Fig.3.10 shows the rear of the PMT whose photocathode was oxidized. One can observe that Kovar glass covering the rear is cracked along the side cover of PMT. The red arrow in Fig.3.10 points the crack from which the air entered, causing the oxidization of photocathode.
From this cooling test, we find that a little difference in thermal expansion characteristics between a filler and a rear of PMT results in a serious damage to the PMT when it is cooled down to 165K. Consequently, a filler must not be attached directly to a rear of PMT, and we started to investigate other ways of filling the space.
A spacer which fit nearly into PMT rear is one of ideas we are now considering. It is made of a mixture of STYCAST and quartz glass, and the electric parts on base circuit is filled in with tight clearance. Fig.3.11 shows the design of this spacer.
Another idea is to use a spacer made of Derlin. This time, a spacer is machined and no adhesive is used for filling the space, so that PMT rear and electric parts on base circuit is free from stress due to thermal expansion. Fig.3.12 shows the design of this spacer.

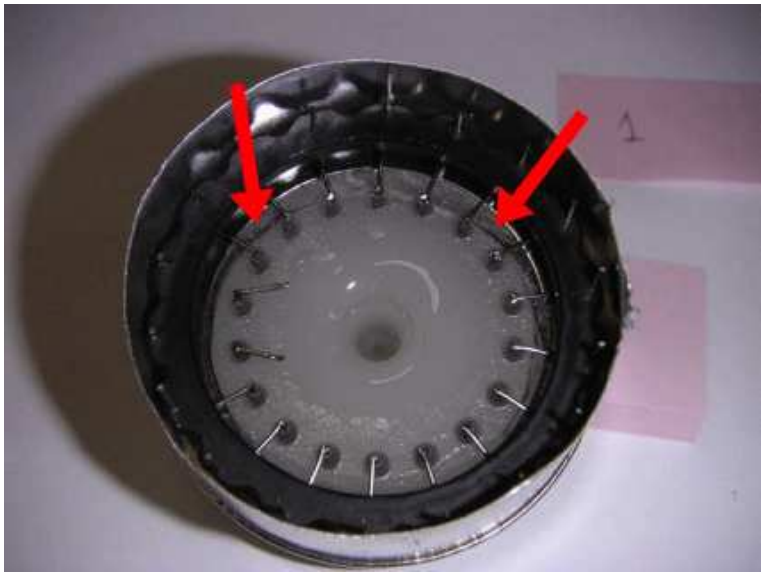

Figure 3.10: The rear of PMT whose photocathode was oxidized

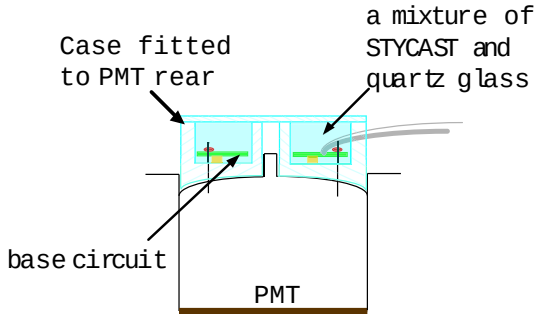

Figure 3.11: A spacer made of a mixture of STYCAST and quartz glass

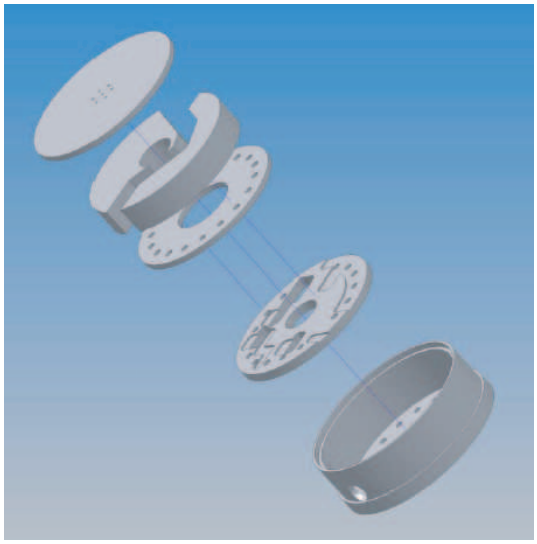

Figure 3.12: A spacer made of Derlin

Chapter 4

Summary

1. R&D studies of the photomultiplier for MEG Liquid xenon Calorimeter have finished and photomultiplier operational in liquid xenon with high quantum efficiency is now available.

2. We made a PMT Test Facility at ICEPP, Univ. of Tokyo. We have succeeded in liquefying and maintaining xenon stably in Small xenon Chamber. With this facility, PMTs can be tested in liquid xenon so that their cryogenic performances can be investigated.

3. Rate dependence of PMTs was investigated using Small xenon Chamber. It was analyzed from two points of view; the photocathode tolerance to high rate background environment and the stability of PMT gain. We confirmed that the photocathode of final version PMT will maintain its stability within $\pm 1\%$ (full width) until the level of high rate background reaches 1.0×10^7 photoelectrons per sec. The PMT gain is stable within $\pm 1\%$ up to 0.5μ [A] in terms of average anode current. The photocathode tolerance to high rate background environment is found to be adequate for the operation of calorimeter.

4. We started R&D studies on second version PMT base circuit where Zener diodes are mounted. With the second version PMT base circuit, it was confirmed that PMT maintains its stability within$\pm 1\%$ until the level of high rate background reaches 5μ [A] in terms of average anode current. However, a problem with Zener diode was found, a large amount of noise generated by Zener diode. We also found out that the noise from Zener diode affect signal output of PMT. Though a rough study shows that this noise will not affect the resolution of calorimeter, a careful study on this noise is needed. For instance, with waveform analysis, it is able to discriminate the noise from signals of γ events.

5. We did R&D studies on filling the space between the PMT rear and the calorimeter wall. We investigated material for the filler and the way of filling the space. The first idea was to attach a low-viscosity adhesive to the space, which was found to be not a good idea. A little difference in thermal expansion characteristics between a filler and the PMT rear causes a serious damage to PMT. Another way of filling the space is now being investigated.

Acknowledgment

First of all, I thank my adviser Prof. Toshinori Mori for his guidance throughout my past two years. I also thank Prof. Satoru Yamashita for always giving me useful advises and encouragement. Perhaps none of my works could have been done without them.
Dr.Satoshi Mihara, Dr.Wataru Ootani and Dr.Toshio Nanba were generous to teaching me many experimental techniques. I must also thank them.
I would like to express my gratitude to Prof. Tomiyoshi Haruyama for his advice on cryogenics techniques.
Mr.Kenji Ozone and Mr.Hajime Nanjo taught me hundreds of things and provided me with many new ideas. I thank them so much.
Mr. Atsushi Yamaguchi helped me so much with various PMT tests in ICEPP. Beside the Small Xenon Chamber, we sat up all night liquefing Xe and discussing physics. I'd like to express my appreciation for his kind help.
To all members in the MEG Collaboration, especially Dr.Toshiyuki Iwamoto, Dr.Shuei Yamada, Mr.Hajime Nishiguchi, Mr.Ryu Sawada, Mr.Hiroaki Natori, Mr.Yusuke Uchiyama and Mr.Takuya Kotajima, I would like to render thanks for their continuous support.
I also thank Mr.Mitsuhiro Tanaka for his warm support. He made a lot of apparatus for this experiment. I am really amazed at his expert craftsmanship.
Finally and foremost, I really thank my parents for their kind and generous supports. They have provided me with their profound love, encouragement, and understanding. There are no words to express the gratitude that I owe them. Thank you so much.

Bibliography

[1] T.Mori et al. Research Proposal to PSI, May 1999

[2] J.Hisano and D.Nomura, Phys. Rev. D59(1999) 116005

[3] T.Doke et al. NIM A 327(1993) 144

[4] T.Iwamoto et al., JPS 2004 autumn meeting; Transparencies are available at http://meg.web.psi.ch/docs

[5] Photomultiplier Tube Accessories ; available at http://usa.hamamatsu.com/en/home.php

[6] Data sheet of NEC Zener diode; available at http://www.necel.com/nesdis/image/D11444EJ5V0DS00.pdf

[7] Makoto Minowa et al. NIM A 320(1992) 500